



Late Weichselian and Holocene climatic and local controls on aeolian deposition inferred from decomposing grain size-shape distributions



Johannes Albert van Hateren ^{a, b, *}, Cornelis Kasse ^a, John van der Woude ^a,
Jeroen Schokker ^c, Maarten Arnoud Prins ^a, Ronald Theodorus van Balen ^{a, c}

^a Faculty of Science, Department of Earth Sciences, Vrije Universiteit, Amsterdam, 1081, HV, the Netherlands

^b VHGM, Mariastraat 44, 2181, CV, Hillegom, the Netherlands

^c TNO-Geological Survey of the Netherlands, Utrecht, 3584CB, the Netherlands

ARTICLE INFO

Article history:

Received 24 December 2021

Received in revised form

27 April 2022

Accepted 30 April 2022

Available online 19 May 2022

Handling Editor: Mira Matthews

Keywords:

Quaternary

Paleoclimatology

Paleoenvironmental reconstruction

Western Europe

Sedimentology-loess

Aeolian stratigraphy

Vegetation dynamics

End-member modelling

Grain size-shape distributions

Aeolian sediment transport mechanisms

ABSTRACT

Aeolian deposits form rich archives of climatic and environmental changes, which have not been fully explored. In this study, results from end-member modelling of grain size-shape distributions were combined with palynological records to reconstruct sedimentary environments and transport mechanisms, and to distinguish climatically-caused from local or system-intrinsic variabilities. We compare results from Weichselian aeolian type locality Lutterzand in the Eastern Netherlands to those of a aeolian site in the Central Netherlands. Four grain size-shape end-members were determined. These represent coarse fluvial or aeolian bedload, fine aeolian bedload, aeolian modified saltation and aeolian suspension (loess) transport mechanisms. We assume that synchronous changes in end-member composition at the two sites are effects of climate change; non-synchronous changes are the result of local or system-intrinsic variability, which are attributed to the influence of the paleo-topographic position on local humidity of the sediment bed. Our results show that during the final stage of the Late Pleniglacial, a change from polar desert to wet sand-sheet paleo-environment occurred, which implies increased humidity and decreased wind speed that may be linked to a northward shift of the polar front preceding warming during the Bølling time interval. The deposition of loess during the Bølling implies further climate amelioration and a concomitant increase in vegetation density. The landscape re-opens during the Older Dryas. The high degree of sediment sorting and near absence of modified saltation and suspension transport mechanisms/end members during this phase are indicative of an undulating aeolian topography and the formation of incipient dunes, for which sparse vegetation forms growth nuclei. A high loess content reveals that the *Betula* phase of the Allerød was humid. The subsequent Allerød *Pinus* phase was drier, potentially due to *Pinus*-induced drought and wildfires. The deposits of the Younger Dryas reflect a paleo-environment similar to that of the Older Dryas. Land use-induced sand-drifting in the Middle Ages is differentiated from the Late-Weichselian aeolian depositional phases by a higher proportion of suspension and modified saltation end members, reflecting wetter climate and denser vegetation during the Holocene.

© 2022 The Authors. Published by Elsevier Ltd. This is an open access article under the CC BY license (<http://creativecommons.org/licenses/by/4.0/>).

1. Introduction

During the last glacial and the transition to the Holocene, a large belt of periglacial sandy aeolian and fluvio-aeolian deposits was

formed in Eurasia (Fig. 1A), spanning from Eastern Great Britain (Bateman, 1995, 1998; Murton et al., 2003), across Belgium and the Netherlands (De Moor, 1981; Koster, 1988; Kasse, 2002), Germany and Poland (Küster et al., 2014; Manikowska, 1991; Zieliński et al., 2015), the Baltic states, Finland, Belarus and Ukraine (Zeeberg, 1994, 1998; Molodkov and Bitinas, 2006; Kalińska-Nartiša et al., 2016; Stańcikaitė et al., 2011; Zieliński et al., 2015) to Russia (Drenova et al., 1997; Matlakhova, 2015; Zeeberg, 1998). Part of the deposits cover pre-existing morphology, leading to the well-known term “coversands”. However, the belt is morphologically diverse

* Corresponding author. Faculty of Science, Department of Earth Sciences, Vrije Universiteit, Amsterdam, 1081, HV, the Netherlands.

E-mail addresses: hvhateren@gmail.com (J.A. van Hateren), c.kasse@vu.nl (C. Kasse), j.d.vander.woude@vu.nl (J. van der Woude), jeroen.schokker@tno.nl (J. Schokker), m.a.prins@vu.nl (M.A. Prins), rt.van.balen@vu.nl (R.T. van Balen).

and comprises dunes. We therefore use the broader term sandy aeolian deposits or sandy aeolian belt. These deposits are an important terrestrial archive of late Weichselian landscape and climate conditions. However, with the exception of deposits or soils associated with the Bølling-Allerød warm phase, they generally lack sufficient organic material for methods such as pollen analysis and macro-remains analysis (Van der Hammen and Wijmstra, 1971; Kasse, 2002). East of Poland, the amount of pollen and macro-remains in Bølling-Allerød paleosols is generally insufficient for reliable vegetation reconstruction (Vorobieva et al., 2021). Thus, the reconstruction of paleo-environments and climatic conditions in sandy aeolian environments mainly relies on morphology, sedimentary facies and grain-size characteristics.

Ambiguity arises because most deposits are mixtures of different sediment populations derived from different sources and transported to the site of deposition by different transport mechanisms (e.g. Prins and Weltje, 1999; Weltje and Prins, 2003). For example, a sediment sample may comprise several laminations, consisting of loess derived from a distant source and bedload derived from a nearby source. When a reconstruction is based on the characteristics of such a 'mixed sample', extremes are lost in translation. Finally, since the transport mode (bedload, modified saltation or suspension) cannot be determined unequivocally using the traditional grain size-based methods (e.g. median grain size or end-member modelling of grain-size distributions), paleo-environmental reconstructions become uncertain (Van Hateren et al., 2020).

The objective of this study is to improve paleo-environmental reconstructions and related climate conditions from (fluvio-) aeolian deposits. We employ end-member modelling on grain size-shape distributions (Van Hateren et al., 2020), which is a form of statistical unmixing that can be used to retrieve information from sediment supplied by multiple transport processes (a 'mixed' sediment in the sense of Weltje and Prins, 2007). In comparison to unmixing based only on grain size distributions, end-member modelling of grain size-shape distributions results in a more accurate determination of the aeolian transport modes because these modes are fingerprinted by their distinct *shape* of the grain size-shape distribution (Van Hateren et al., 2020). To distinguish between climatically caused and local or system-intrinsic variabilities, we compare changes in sedimentary facies and vegetation cover over time of two sites. The first site is Lutterzand, which is the type locality for sandy aeolian stratigraphy located in the Eastern Netherlands (Van der Hammen and Wijmstra, 1971). The second site, Leusden, is situated on a sandy aeolian plateau fringing a Saalian ice-pushed ridge in the Central Netherlands (approximately 100 km west of Lutterzand) (Fig. 1B).

2. Geological setting, aeolian stratigraphy and sedimentary facies

2.1. Geological and geomorphological setting

The sandy aeolian deposits in the Netherlands are part of the European sandy aeolian belt (Kasse, 2002). This belt is roughly confined between the southern limit of the Weichselian ice sheets and the northern limit of the loess belt and/or the continental European mountain ranges (Fig. 1A). The adjoining loess belt was deposited as the distal component of the same aeolian system (Bokhorst et al., 2011; Lehmkuhl et al., 2016; Parks and Rendell, 1992). Overlap occurs between the two belts, as both sandy aeolian deposits and loess may occur at a given site (e.g. Murton et al., 2003; Schokker et al., 2007). Based on heavy mineral

analyses and lateral changes in grain size, the main sources of the fluvio-aeolian and aeolian deposits in the Netherlands are the sediments of the Rhine and Meuse delta plains and the (pro-)glacial deposits along the Pleistocene glacial limits, supplemented by local sources (Kasse, 2002; Schokker et al., 2005). Additionally, the Late Glacial aeolian deposits partially consist of reworked older sandy aeolian deposits (Kasse, 2002).

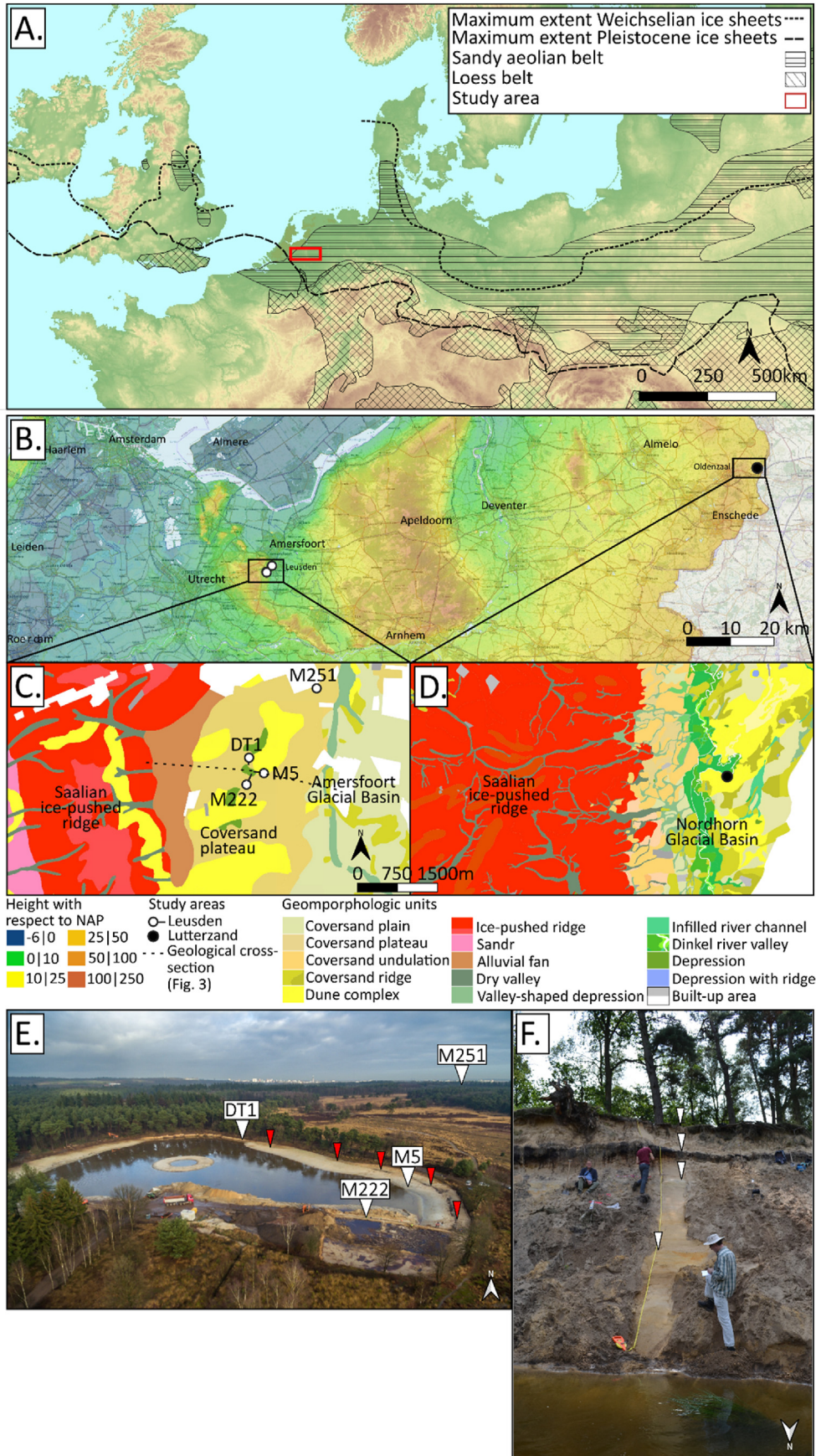
Site Lutterzand lies within a geomorphologically varied fluvial, fluvio-aeolian and aeolian infill of the Nordhorn Glacial Basin (Van der Hammen and Wijmstra, 1971). Exposures were created by incision of the river Dinkel into the deposits (Fig. 1B, D and 1F). The location of our sediment profile is approximately equal to that of profile 1 of Van der Hammen and Wijmstra (1971) and profile 4 of Vandenberghe et al. (2013). However, the sediments in the lower part (up to ~27.2 m) were not investigated by Vandenberghe et al. (2013) due to poor exposure and a higher water level in the river Dinkel. This part of the studied profile is similar to the lower part of profile 3 in Vandenberghe et al. (2013).

The Leusden site comprises several sediment profiles and pollen sections on an undulating sandy aeolian plateau that fringes a Saalian ice-pushed ridge (Fig. 1B, C and 1E). Sediment profile M5 and pollen section M222 are located in a local depression (Fig. 1C; Fig. 2). Sediment profile DT1 is located on the edge of the same depression, whereas sediment profile M251 is located on the slope between the sandy aeolian plateau and the bordering valley (Fig. 1C; Fig. 2). The sediments and pollen of the Leusden dataset were studied in the context of the discovery of a buried Allerød pine woodland (Bazelmans et al., 2021).

2.2. Aeolian stratigraphy in the Netherlands

The classic lithostratigraphic subdivision of the sandy aeolian deposits in the Netherlands was devised at Lutterzand. Marker horizons associated with the Bølling-Allerød warm phases (Lower Loamy Bed and Usselo Soil) and a widespread desert pavement (Beuningen Gravel Bed) enable a subdivision into lithostratigraphic units (Van der Hammen and Wijmstra, 1971, Table 1; for a visual representation see Fig. 3). However, elsewhere this subdivision cannot always be made due to absence of these marker horizons. In the lithostratigraphy of the Netherlands the periglacial deposits of the Late Weichselian are therefore subdivided to a lesser degree (Schokker et al., 2007; TNO-GSN, 2021, Table 1).

The Mekkelhorst Member (unit MHM) is a Middle-Pleniglacial fluvial deposit (Van der Hammen and Wijmstra, 1971; Van Huissteden, 1990). The overlying Older Coversand I (unit OCI) is a Late Pleniglacial fluvio-aeolian deposit which was strongly disturbed by liquefaction and loading due to seasonal freeze-thaw cycles and permafrost degradation (Vandenberghe, 1988; Vandenberghe et al., 2013). The Beuningen Complex (unit BC) was also deposited during the Late Pleniglacial and consists of two subunits. The lower part of the Beuningen Complex is fluvial, occurs locally and consists of shallow gully fills, composed of coarse sand. These gullies truncate unit OCI. The upper part is an aeolian desert pavement which consists of a single or multiple gravel beds with varnish coating and ventifacts, with or without aeolian mantle below (Van Huissteden et al., 2000, 2001; Kasse et al., 2007). The unit comprises both erosive and accretionary elements. It truncates unit OCI and the fluvial Beuningen and is associated with an arctic soil showing translocation of iron (Van der Hammen and Wijmstra, 1971; Vandenberghe et al., 2013). Frost cracks and small sand wedges are occasionally observed to extend downward from the desert pavement (Van Huissteden et al., 2000). The aeolian Older Coversand II (unit OCII) was deposited around the Late Pleniglacial/



Late Glacial transition (Van der Hammen and Wijmstra, 1971; Vandenberghe et al., 2013).

The Lower Loamy Bed (unit LLB) is a silty loess-like deposit formed during the Bølling (Vandenberghe et al., 2013; Van Geel et al., 1989). It is overlain by the Younger Coversand I (unit YCI), a dry aeolian deposit associated with the Older Dryas (Vandenberghe et al., 2013; Van Geel et al., 1989). This unit has a limited thickness in our sediment profile. The Usselo Soil and Loam (unit USL) is an Allerød loess-like deposit that is associated with soil formation and characteristic dung beetle burrows in drier parts of the landscape and peat formation in wetter parts (Van der Hammen and Wijmstra, 1971; Vandenberghe et al., 2013). The overlying Younger Coversand II (unit YCII) is similar to unit YCI and was deposited during the Younger Dryas stadial (Vandenberghe et al., 2013). A podzol soil formed during the Holocene, indicating that sand deposition temporarily ceased. Although the dense vegetation cover of the Holocene strongly inhibited aeolian processes, sporadic dune formation continued throughout the Holocene (Sevink et al., 2018). Widespread aeolian transport was suppressed until humans significantly disturbed the vegetation cover from ~1 ka until recently, causing deposition of Drift Sand (unit DS) consisting of well-sorted aeolian sand deposited by steep-sided dunes (Vandenberghe et al., 2013).

2.3. Stratigraphy of the aeolian deposits near Leusden

Similar to the approach of Van der Hammen and Wijmstra (1971), distinct units of fluvial and aeolian deposition were distinguished for the sandy aeolian plateau based on marker horizons associated with the Bølling-Allerød warm phase and the Beuningen Gravel Bed (BGB; Maarleveld and Van Der Schans, 1961; Westerink, 1981, Fig. 2). The Late Pleniglacial development of the area is relatively similar to that at Lutterzand, except that unit OCI is missing (Westerink, 1981). A desert pavement is recognised on top of Late Pleniglacial alluvial fan deposits (BGB; Westerink, 1981). The aeolian deposits most likely accumulated further east in the Amersfoort glacial basin during this time period (Westerink, 1981, Fig. 2; Fig. 1C). In the earlier work by Westerink (1981) and Maarleveld and Van der Schans (1961), unit OCII and YCI were subdivided based on sedimentary facies. However, without a Bølling marker horizon, the division into units OCII and YCI is uncertain.

The lower organic interval occurring at site M251 and DT1 was dated to the Bølling (Greenland Interstadial 1e) at site M251 (Van Beurden, 2020, Fig. 3). The directly underlying deposits can therefore be assigned to unit OCII. The upper peats at sites M251 and DT1 were dated to the Allerød or early Younger Dryas (unit USL; Bazelmans et al., 2021; Van Beurden, 2020). The aeolian sand between the LLB and USL can therefore be assigned to the Older Dryas and that above the USL to the Younger Dryas. Locally, Holocene drift sands formed (Westerink, 1981). These sediments are not present in the studied sediment profiles.

3. Material and methods

3.1. Sediment sample collection and grain size and shape analysis

To determine grain size and shape, a total of 497 samples were collected of which 247 at Lutterzand and 250 at Den Treek. At Lutterzand, the larger part of the sediment profile was sampled at a vertical resolution ranging between 3 and 5 cm (due to a variable slope of the exposure). A vertical resolution of approximately 1 cm was used for the units LLB-YCI-USL, because these displayed large compositional changes over a small vertical distance (Fig. 3). Sediment profile DT1 of the Leusden site (109 samples) was sampled at a 2 cm vertical resolution, except for the Usselo soil and underlying peat (unit LLB), which were sampled at a 1 cm resolution to capture the abrupt vertical changes occurring in these units (Fig. 3). Sediment profile M5 (50 samples) was sampled at a 1 cm resolution (Fig. 3). In contrast to the ~90° slope at profiles M5 and DT1, the slope of sediment profile M251 was 40–55°. The along-slope resolution was therefore reduced to 5 cm (sandy units) and 2 cm (silts and peats) resulting in 91 samples (Fig. 3). The corresponding vertical sampling resolutions are 3.1–4.4 cm and 1.3–1.6 cm.

Sediment samples of approximately 2 g are pre-treated in ~100 ml demineralised water with 5 ml 30% H₂O₂ to remove organics, 5 ml 10% HCl to remove carbonates and 300 mg Na₄P₂O₇ · 10H₂O to disperse charged particles (Konert and Vandenberghe, 1997). The samples were studied for particle size and shape using a Sympatec Qicpic dynamic image analyser. This analyser is set-up using a 2 mm cuvette. To prevent clogging of the cuvette, pre-treated samples are sieved over a 1600 µm mesh, excluding larger grains from the measurement. Using a stirrer, the sediment is suspended in degassed water and subsequently pumped repeatedly through the measuring zone. Each measurement consists of 5 min of film shot at 25 frames per second, resulting in 15,000 frames per sample. Frames measure 1024 by 1024 pixels of approximately 5 µm wide. The number of sediment particles per measurement depends strongly on the grain size of the sample: the median number of measured particles is approximately 60 thousand, the 10th percentile is 30 thousand (coarse-grained samples) and the 90th percentile is 160 thousand (fine-grained samples).

Image processing is carried out according to the method outlined in Van Hateren et al. (2020). For the current research we use two variables. To describe particle size, we use the area-equivalent diameter (D_{2d}). This is the diameter of a circle that has the same area (A) as the particle: $D_{2d} = 2\sqrt{\frac{A}{\pi}}$. The shape of the particles is represented by convexity, a parameter that describes the irregularity of particles. Convexity (Con) is a ratio between the length of a convex hull around the particle (P_{ch}) and the length of the perimeter of the particle (P_p): $Con = \frac{P_{ch}}{P_p}$. Convexity was used as shape-parameter since it proved to be most effective in determining the aeolian transport mode (Van Hateren et al., 2020). For every sample, the D_{2d} and convexity data were integrated into a grain size-shape distribution (SSD) termed ConD_{2d} (Van Hateren et al., 2020). Due to the dynamic image analyser's pixel size of

Fig. 1. A) Approximate location of our study sites with respect to the Late Weichselian sandy aeolian belt (Kasse, 2002; increased extent in England after Bateman, 1995; Bateman, 1998), loess belt (Lehmkuhl et al., 2016; Bokhorst et al., 2011; Murton et al., 2003; Parks and Rendell, 1992), maximum ice sheet extent (Kasse, 2002) and elevation (European Environment Agency, 2020). The sandy aeolian belt depicts the area where predominantly sandy aeolian deposits are found at the surface. B) Location of study sites Leusden (central Netherlands) and Lutterzand (eastern Netherlands). Source of topographical map: © J.W. van Aalst, www.opentopo.nl (June 30, 2020). Elevation is with respect to the Dutch ordnance datum (NAP). Source of elevation map: AHN2 © PDOK.nl, 2020a, 2020b (June 30, 2020). C) Geomorphological map of site Leusden. D) Geomorphological map of site Lutterzand (source of geomorphological maps: Geomorfologische Kaart Nederland 1:50,000, © PDOK.nl). E) Photograph of the depression at Leusden formed by sand mining with outcrops DT1, M5 and M222. View direction is towards the North (photograph courtesy of Cultural Heritage Agency of the Netherlands). The approximate location of sediment profile M251 is also shown. Red triangles show outcropping of the Allerød peat/Usselo soil (upper organic interval). F) Photograph of the outcrop at Lutterzand. From bottom to top, white triangles point towards: Beuningen gravel bed discordance, Usselo soil, Holocene podzol, current surface. (For interpretation of the references to colour in this figure legend, the reader is referred to the Web version of this article.)

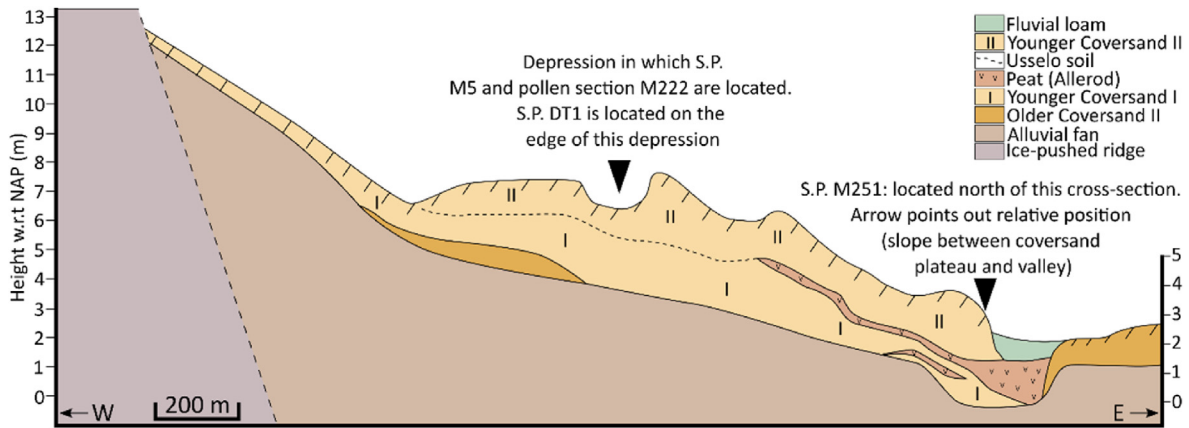


Fig. 2. Geologic cross-section redrawn after Westerink (1981) with (relative) positions of sediment profiles (S.P.) and pollen section M222. The position of this cross-section is shown in Fig. 1C.

Table 1

Lithostratigraphy and age of the (fluvio-)aeolian deposits. The age and the classic units are based on the deposits at Lutterzand. From left to right the columns show: 1) The lithostratigraphic framework of the Netherlands after Schokker et al. (2007) and TNO-GSN (2021), 2) Classic lithostratigraphic units defined for Lutterzand by Van der Hammen (1951), Van der Hammen and Wijmstra (1971) and Van Geel et al. (1989), 3) age intervals for the classic units defined at Lutterzand (OSL ages from Vandenberghe et al., 2013 except if noted otherwise, MAO = minimum age of onset of deposition (bottom of unit not sampled), MAED = maximum age of the end of deposition (top not sampled due to truncation by next unit)), 4) the biochronozones associated with the classic units (Van der Hammen and Wijmstra, 1971; Hoek, 1997 A), and 5) the relationship between biochronozones and the Greenland Ice-core Event Stratigraphy (Late Glacial after Hoek and Bohncke, 2001; Pleniglacial and Holocene after Rasmussen et al., 2014).

Lithostratigraphic unit	Classic unit	Age (ka)	Associated biochronozone	Associated Greenland Ice-core Event
Boxtel Formation (Kootwijk Member)	Drift Sands (DS)	0.2 ± 0.02–0.4 ± 0.04	(Late) Holocene	Holocene
Boxtel Formation (Wierden Member)	Younger Coversand II (YCII)	12.2 ± 0.9–13.6 ± 1.1	Late Glacial	Younger Dryas
	Usselo Soil and Loam (USL)	12.7 ± 0.9–14.8 ± 1.2. Radiocarbon age (Vandenberghe et al., 2013) 13.2 ± 12.9 cal BP	Allerød	Greenland Interstadial 1a to 1c
	Younger Coversand I (YCI)	14.8 ± 1.2	Older Dryas	Greenland Interstadial 1d
Boxtel Formation (undifferentiated)	Lower loamy Bed (LLB)	13.8 ± 1.0–15.7 ± 1.3. Bølling interstadial, based on pollenstratigraphy (Van der Hammen and Wijmstra, 1971)	Bølling	Greenland Interstadial 1e
	Older Coversand II (OCII)	12.3 ± 1.0–15.2 ± 1.2	Late Pleniglacial	Greenland Stadial 2 and 3 and intervening Interstadial
	Beuningen Complex (BC)	Fluvial Beuningen: 16.1 ± 1.3–23.5 ± 1.8 Beuningen Gravel Bed: ca 14–16		
	Older Coversand I (OCI)	19.9 ± 1.6 (MAED) - 25.2 ± 1.9 (MAO) (17.2 ± 1.2–25.2 ± 2.0 ka at Grubbenvorst in S Netherlands (Kasse et al., 2007))		
	Mekkelhorst Member (MHM)	Circa 26–55 ka (Van Huissteden, 1990)	Middle Pleniglacial	Greenland Interstadial 3–17 and intervening Stadials

approximately 5 μm, a reliable measurement of particle shape is not possible for particles that are finer than 13 μm (Shang et al., 2018; Van Hateren et al., 2020) which are therefore excluded from the analyses. Literature suggests that this fraction is of limited importance in the studied (fluvio-)aeolian deposits (e.g. Vandenberghe et al., 2013).

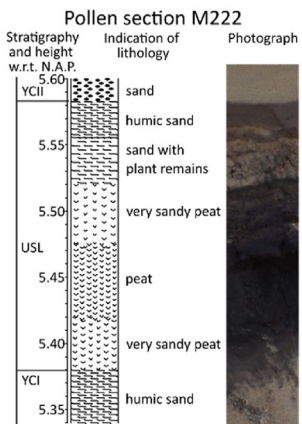
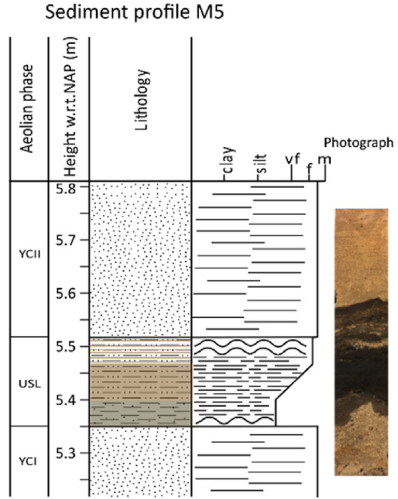
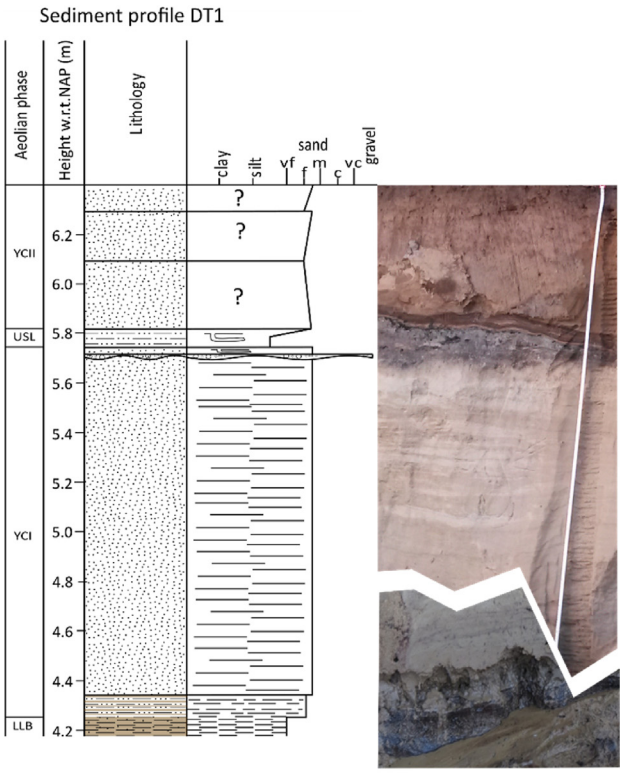
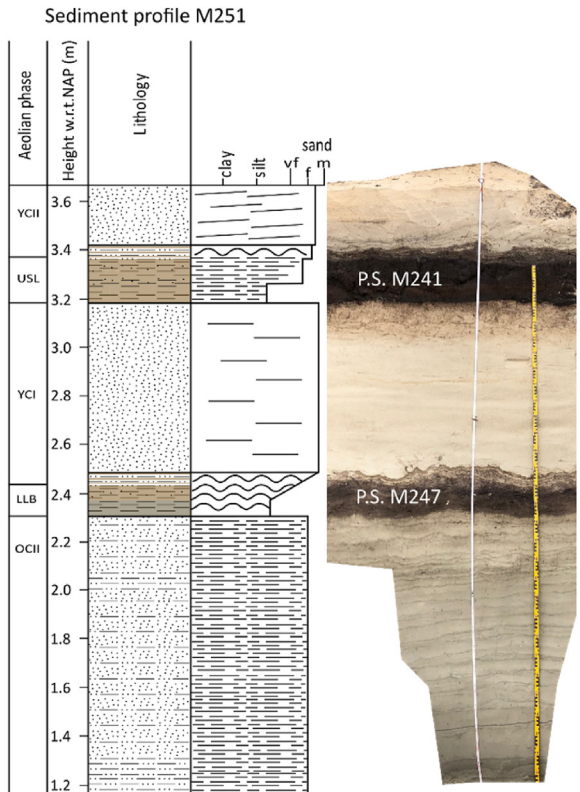
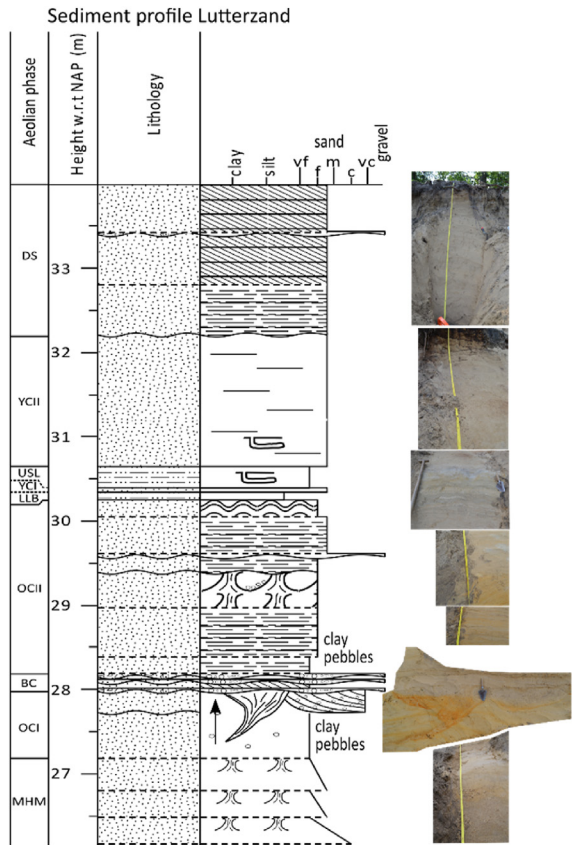
3.2. Data processing

End-member modelling of the combined SSD datasets of Leusden and Lutterzand is performed with the AnalySize algorithm (Paterson and Heslop, 2015) because its output is most accurate amongst the available algorithms (Van Hateren et al., 2018). The fit of end-member modelling outcomes to the size-shape distribution dataset is given by variance squared (R^2 , coefficient of determination). This fit is used to deduce the number of end members needed to adequately describe the dataset. Two types of R^2 are used: 1) class-wise R^2 , which indicates the fit per grain size class (grain-size distributions) or grain size-shape class (SSDs), and 2) Sample-wise

R^2 , which signifies the fit per sample (Van Hateren et al., 2018, 2020).

3.3. End-member verification samples

To determine the geological significance of the modelled end members, ten samples with observed sedimentary structures were obtained from Lutterzand. The sedimentary structures allow a direct interpretation of the depositional processes and environment. The SSDs of these end-member verification samples were compared to the end-member modelling outcome. We obtained a sample of the silt and fine sand grains in a peat that is a lateral equivalent of the Usselo soil (profile 1 of Vandenberghe et al., 2013). At our main section we obtained one sample of the sediment in the shallow channel structures associated with the fluvial part of the Beuningen complex, two samples of the sediment in granule ripples (45 and 61 cm above the lowermost thin gravel bed of the BGB), one sample of the sediment in the upper BGB thin gravel bed, one sample of the sediment associated with low-angle cross-



bedding (incipient or dome-shaped dune), one sample of a loam band below the LLB and one sample of the loam in the LLB (Fig. 3). We have avoided the thin sandy intercalations in the loam in order to obtain a pure loess reference sample. Two additional samples were obtained approximately 130 m to the East-Northeast from our main study site, in the cutbank of the first downstream meander bend. These comprise a third loam sample from the LLB and a sample from the sediment associated with adhesion ripples, which form under humid bed conditions (Hunter, 1980).

3.4. Palynology

Pollen analysis is used to establish a biochronostratigraphic framework (mainly dependent on the arboreal to non-arboreal pollen ratio and changes in the tree species) and to reconstruct the depositional environment based on the local and regional palaeovegetation. We therefore use concise pollen diagrams consisting of trees, shrubs and a selection of herbs. Two humic layers at Leusden sediment profile M251 were collected in box cores (sample code of the lower layer: LESN18-M247; sample code of the upper layer: LESN18-M241, hereafter M247 and M241) (Fig. 3). Pollen samples of circa 1 cm³ were obtained at a 2 cm resolution from box cores M247 and M241 and at a 1 cm resolution from box core M222. At Lutterzand, five consecutive samples, each 1–3 cm thick, together cover the entire aforementioned peat that is the lateral equivalent of the Usselo soil (profile 1 of Vandenberghe et al., 2013). In the laboratory, the large-volume samples were mixed prior to pollen analysis.

Pre-treatment was carried out according to Faegri and Iversen (1989). After a first scan in order to estimate the quality and density of the pollen, most of the pollen slides of M241, half of those of M247 and two-thirds of those of M222 were analysed under a light microscope. Beug (2015) was the main reference for identification. We aimed for a pollen sum (trees + shrubs + upland herbs) of at least 200, but this was not always possible. Pollen diagrams were prepared using the Tilia software for paleoecological data (Grimm, 2004). Visibility of the curves of minor species is enhanced by adding a shading where the number of pollen was multiplied by 7. Zonation in the pollen diagrams is done visually and zones are numbered according to Hoek (1997 A). The Dutch national database of flora and fauna (Nationale database flora en fauna, 2020) and Collins Wild Flower Guide (Streeter, 2016) are used for ecological interpretation of specific taxa.

4. Results

4.1. Sediment characteristics

The sediment characteristics and bedding type at Lutterzand, as shown in Fig. 3, have been described in-depth by previous authors for the current and surrounding sediment profiles (Van der Hammen and Wijmstra, 1971; Van Huissteden, 1990; Vandenberghe et al., 2013). In addition to the previous work we observed clay pebbles and flat channel structures in the lower part of the OCII unit, loading structures in the middle part of the unit and a concentration of crinkly-laminated loam laminae below the LLB (Fig. 3).

The sediment characteristics of the sediment profiles at Leusden have not been presented in previous work, except for the Allerød succession at M5, which was described in the context of a study

into a buried pine forest (Bazelmans et al., 2021). Unit OCII in sediment profile M251 shows horizontally alternating bedding of loamy fine sand and fine sand (Fig. 3). Similar to the sediment profile at Lutterzand, a concentration of crinkly laminated loam laminae is present below the LLB (Fig. 3). The bedding of the LLB at profile DT1 could not be studied in detail because the unit was located near the groundwater table (Fig. 3). At profile M251, the unit comprises two horizons that together form a coarsening-up sequence: the base consists of a grey organic loam and the top of a blackish-coloured organic fine sand (Fig. 3; Fig. 9). The unit becomes increasingly involuted towards the top (Fig. 3). The transition to unit YCI is marked by alternations of organic-poor and organic-rich sand laminae (Fig. 3). The remainder of the YCI deposits lack loamy laminae and have a homogeneous grain size (Fig. 3; Fig. 9). Several additional (sedimentary) structures are observed laterally from the sediment profiles: An ice-wedge cast (near profile DT1; Appendix A1), lenses with cross-bedding (near profile DT1; Appendix A2) and a dome-like dune structure (near profile M251; Appendix A3). Similar to Lutterzand, the Allerød is characterised by peat and silt accumulation on the humid parts of the terrain: the valley axis, the slope towards the valley axis and the local depressions (Fig. 2; Fig. 3). The dry parts of the terrain are characterised by silt accumulation and formation of the Usselo soil with characteristic dung beetle (*Typhaeus typhoeus*) burrows and a bleached horizon (Fig. 2; Fig. 3).

Similar to unit YCI, the base of unit YCII in all our sediment profiles except DT1 is marked by alternating laminations of sand and sand with organic remains, and by small-scale involutions (Fig. 3). The remainder of unit YCII consists predominantly of horizontally to low-angle bedded fine to medium sand. At DT1 the bedding is not visible due to illuviation from the overlying Holocene podzol (Fig. 3).

4.2. The statistically feasible number of end members in the size-shape distribution dataset of Leusden and Lutterzand

Distributions of class-wise R² indicate the extent to which outcomes with different numbers of end members reproduce size-shape variability in the dataset (Fig. 4).

A model with only one end member cannot reproduce any variability (1 EM, Fig. 4). The result with two end members increases model fit significantly but lacks explanatory power around a grain size of 180–250 μm. Addition of a third end member results in improvement of the fit to this size fraction and the silt fraction (<~63 μm). However, the irregularly shaped sediment grains remain poorly explained by the model (below a convexity of ~0.93). Addition of a fourth end member further improves the fit within the region with significant amounts of data (white contour line), especially at a grain size of ~125 μm and a convexity of ~0.95. Thus, the 4 EM solution is able to reproduce the bulk of the size-shape variability in the dataset (Fig. 4).

The 5 EM solution slightly improves the fit to the irregularly-shaped fraction of the sediment. Further increasing the number of end members does not result in a significant increase in fit to the size-shape classes (Fig. 4). Moreover, solutions with more than 6 end members improve fit by including the noisy coarse range above ~600 μm. Results in this range are not statistically robust because the volume consists of a few large grains distributed over the available grain size and shape classes (compare Figs. 8 and 9 with Fig. 4). In conclusion, a minimum of four end members is required

Fig. 3. Sedimentary logs of the study sites with photographs of the section shown below. Stratigraphical correlation denoted by abbreviated unit names. For locations see Fig. 1. The black arrow in the sedimentary log of Lutterzand indicates where samples were taken in unit OCII. Pollen section (P.S.) M241 and M247 were obtained from the organic intervals at site Leusden-M251 (see photograph). The lithology of pollen section M222 is simplified and no bedding is shown because the section has only been used for pollen analysis and was not part of the detailed lithological and sedimentological study.

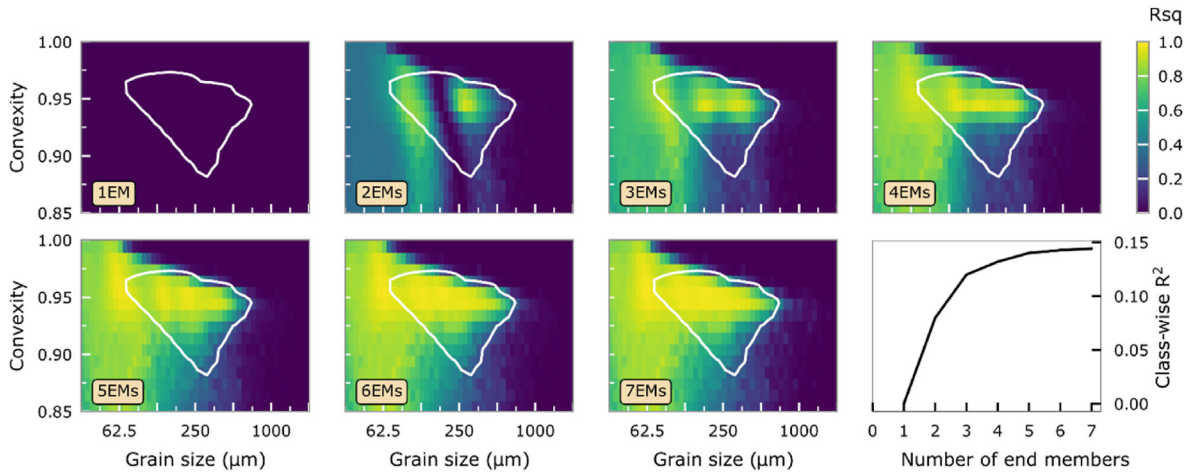


Fig. 4. Class-wise R^2 distributions for end-member modelling results of the combined Cond2d distribution dataset. Statistics are shown for outcomes with one to seven end members. The white line traces the 97.5th percentile of the median SSD of the dataset. In other words, 97.5% of the volume of the 'average' distribution lies within the white line. The panel on the lower right shows the average class-wise R^2 versus the number of end members.

to fit most size-shape classes with significant data satisfactorily. The fit of end-member modelling outcome to the data can also be expressed as fit per sample (sample-wise R^2 ; Fig. 5). For all

sediment profiles the fine-grained intervals (LLB and USL units) and coarse-grained samples are characterised by a lower fit. The 1 EM solution shows a significantly worse fit compared to the 2 EM

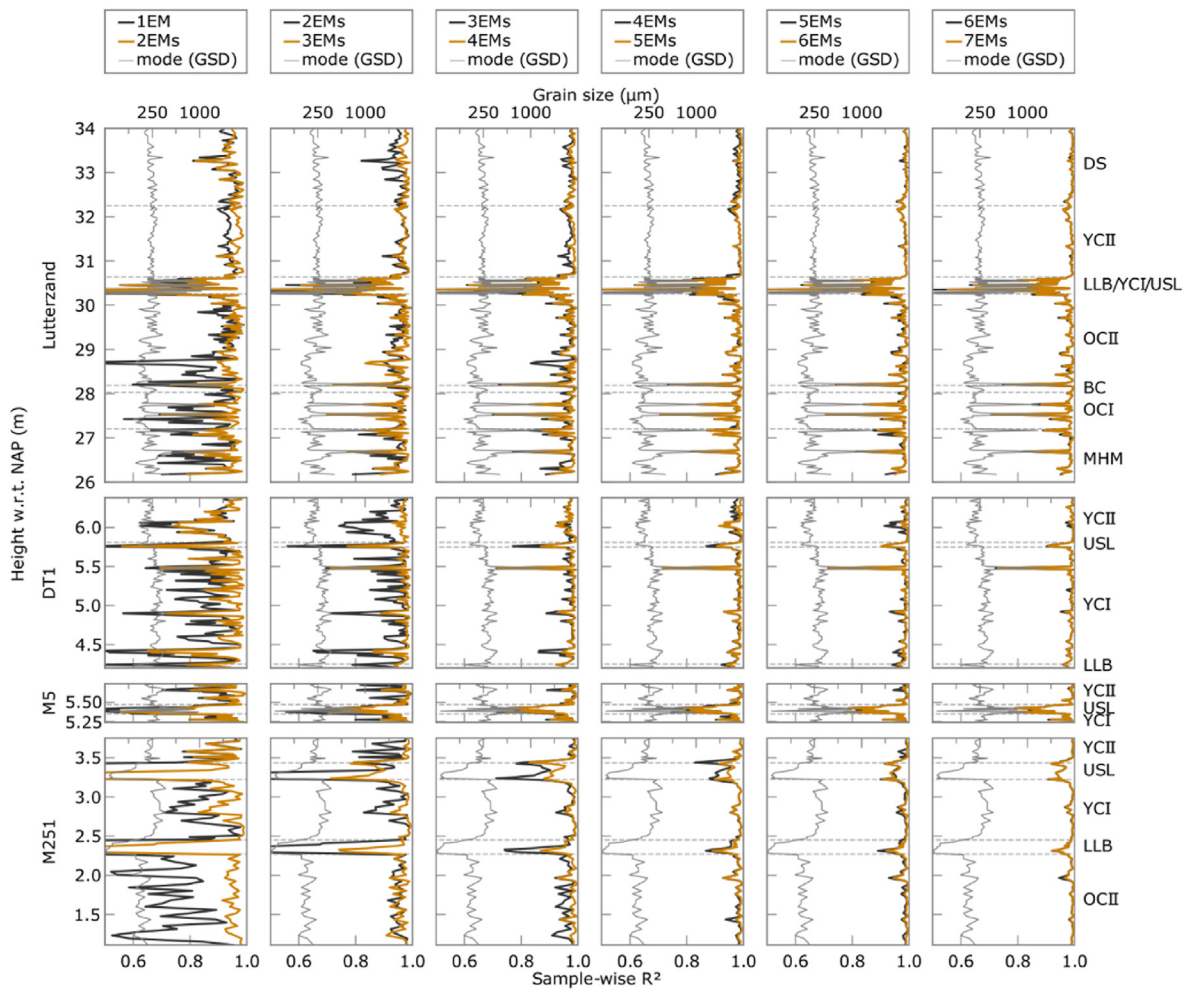


Fig. 5. The fit of the end-member modelling outcomes to each sample. Section names are indicated on the left-hand side and names of the stratigraphic units on the right-hand side. The modal grain size is displayed to indicate the relationship between grain size and model fit.

solution. The 3 EM solution improves fit mainly for the LLB and USL intervals. Addition of a fourth end member results in a slight improvement of fit, especially for the Mekkelhorst Member (lower part of the Lutterzand sediment profile), in OCII, in the lower part of YCII and in the drift sand intervals. A further increase in the number of end members does not improve the fit significantly (Fig. 5).

Similar to the Lutterzand dataset, the fine-grained intervals (LLB and USL units) and coarse-grained samples of the Leusden dataset (profiles DT1, M5 and M251) are characterised by a lower fit of the model (Fig. 5). Compared to the 1 EM solution, a model with two end members improves fit to all units and especially to the OCII interval (M251). The 3 EM solution further improves fit to all units except OCII, whereas addition of a fourth end member mainly improves fit to the OCII, LLB and USL units. Addition of a fifth end member only results in a minor increase of fit to specific samples (Fig. 5). More end members are not statistically feasible.

4.3. Grain size-shape distributions of the four end members and comparison to reference samples

The grain size-shape distributions, the grain size distributions and the grain shape (convexity) distributions of the four end-member outcome are shown in Fig. 6. End-member EM1 consists predominantly of medium sand with a primary mode at 370 µm and a small secondary mode at 125 µm. It is well-sorted in terms of grain convexity (lower row) and the convexity is constant with increasing size (upper row). End member EM2 consists of well-sorted fine to medium sand with a mode at 220 µm and is better sorted in terms of grain size than EM1. It is slightly less sorted in terms of grain convexity. Furthermore, convexity decreases with increasing size. End member EM3 is similar to EM2 in terms of convexity (sorting and trend with increasing size) but is finer-grained (very fine to fine sand with a mode at 155 µm). End member EM4 is significantly finer-grained (silt to very fine sand), shows a strong decrease in convexity with increasing size, and is

poorly sorted in terms of both grain size and grain shape.

The SSDs of the four end members are compared to those of verification samples. Appendix B shows the correlation values between the end members and each reference sample, whereas Fig. 7 shows the end members in comparison to their best-fitting reference samples. EM1 shows highest correlation with sediment associated with aeolian granule ripples and aeolian low-angle cross-bedding, although the correlation value is relatively low because the end member is characterised by a smaller grain size range (better sorting) than the verification samples (Appendix B; Fig. 7). An important similarity between EM1 and the verification samples, including the sediment from the fluvial part of the Beuningen complex, is the constant convexity with increasing size (Fig. 7). EM2 correlates best with the finer sediment fraction of low-angle cross-bedding and the coarser sediment fraction of adhesion ripples. The best-fitting adhesion ripple sediment sample is slightly finer-grained, but shows the same minor decrease in convexity with increasing size. The low-angle cross-bedding sediment sample has a small fraction of coarser grains than observed in the end member. EM3 shows a similar trend in variation of grain shape with grain size as the sediment from adhesion ripples, but the sediment is coarser grained than the end member. EM4 fits well to all samples from the lower loamy bed (loess) as well as to the lithogenic fraction in the peat that is a lateral equivalent of the Usselo soil. However, the reference samples show more volume below ~50 µm and some contain irregularly shaped coarse grains (similar to EM1, EM4 is better sorted than the reference samples).

4.4. Temporal evolution in end-member and vegetation composition at Lutterzand

The Mekkelhorst member (up to circa 27.2 m) is characterised by repetitive alternations of EM1 to EM2 to EM3 (fining-up sequences; Fig. 8). Unit OCI and the basal part of unit OCII (27.2–29 m) are typified by a mixture of all four end-members, but

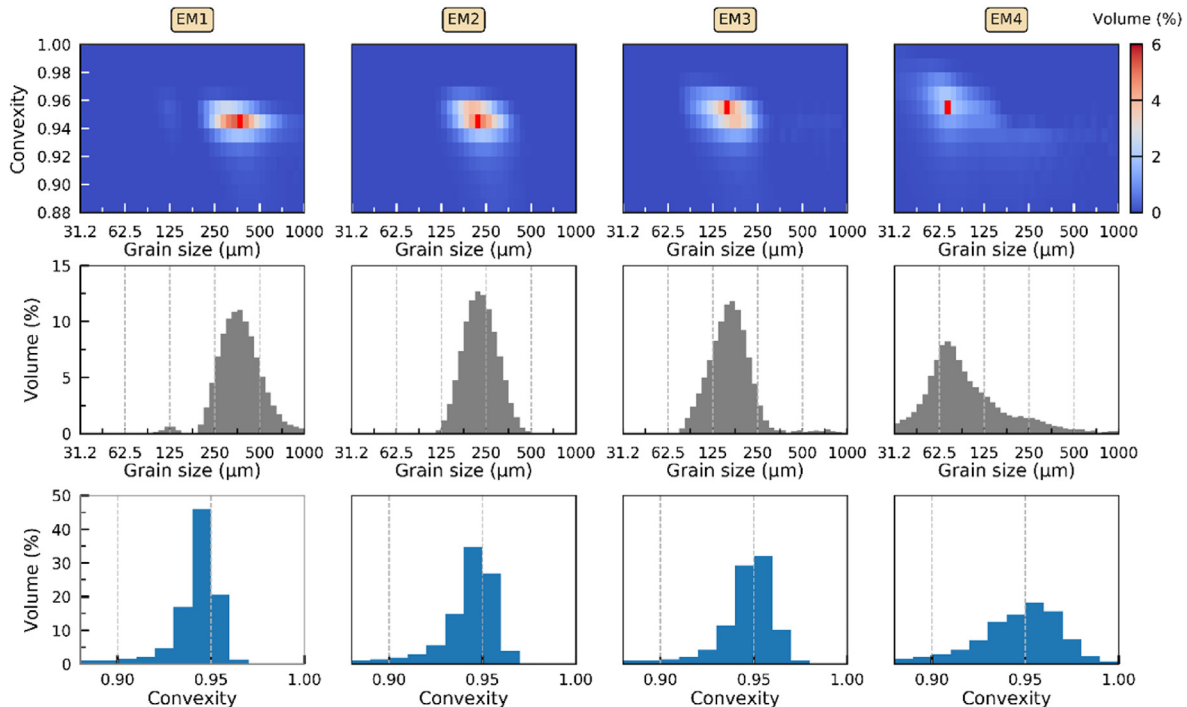


Fig. 6. Grain size-shape distributions of the 4 EM solution. The bright-red squares in the SSDs denote the volumetric peak of the distribution. The grain size and grain-shape distributions of these end-members are shown below to display the sorting in terms of grain size and grain shape. (For interpretation of the references to colour in this figure legend, the reader is referred to the Web version of this article.)

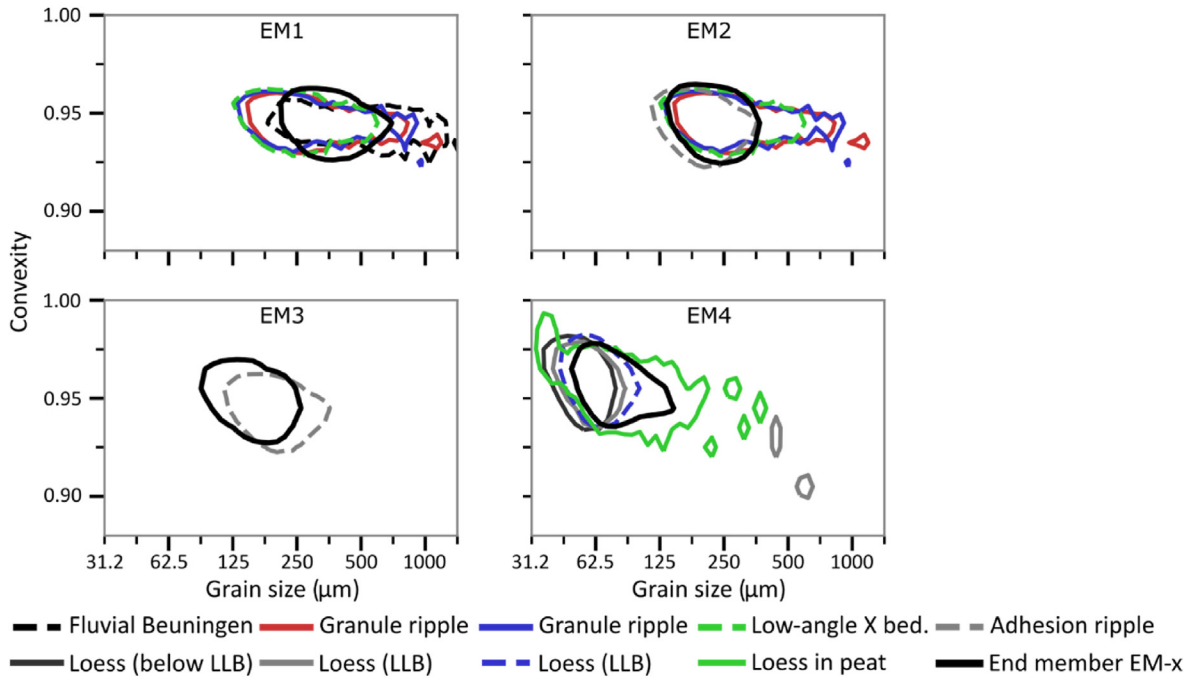


Fig. 7. Contours of the SSDs of the end-members (solid black lines) compared to the best fitting reference samples (legend shown below figure). The contours are drawn along the edge of the SSDs where the size-shape classes contain 0.7% of the total volume. A contour level of 0.2% was used for the 'loess in peat' reference sample because it is poorly sorted and therefore cannot be visualised well using 0.7%.

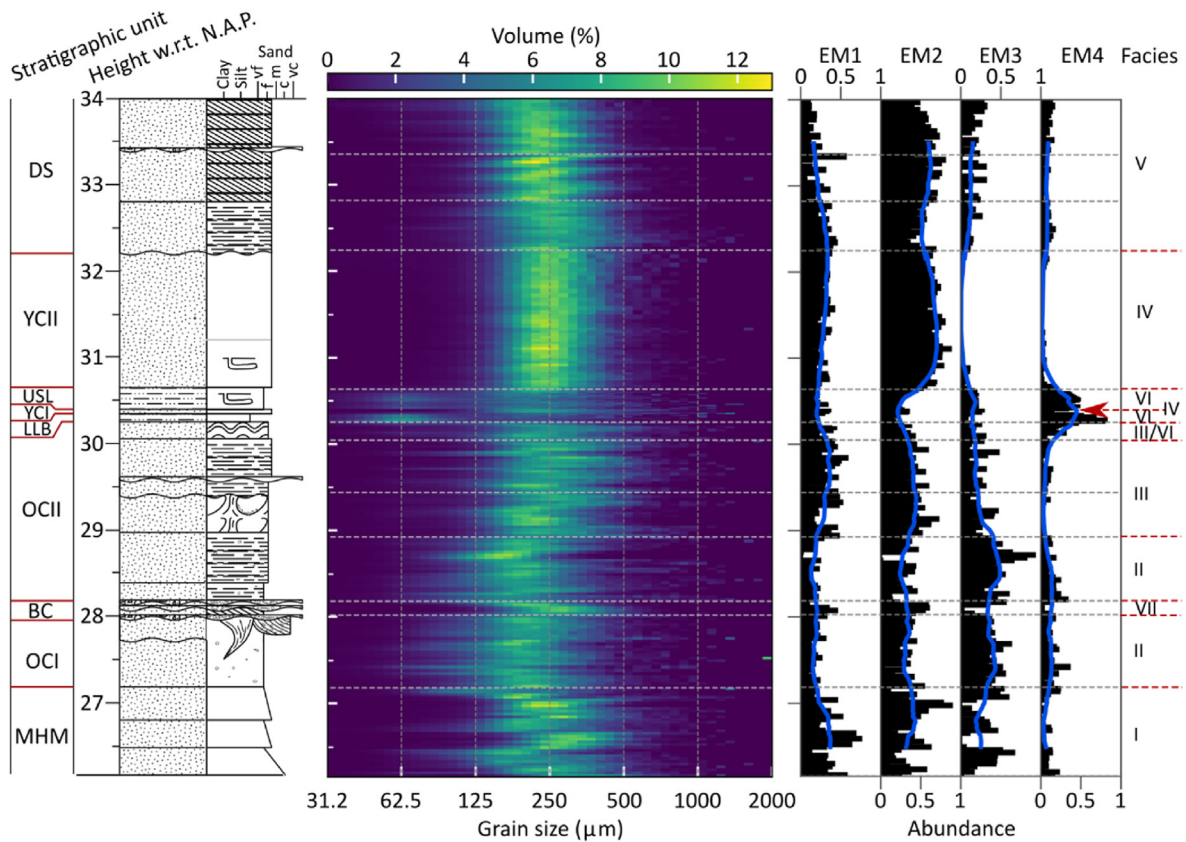


Fig. 8. End-member abundances for the Lutterzand sediment profile with grain-size distributions and a simplified lithologic column for reference. Stratigraphic units as defined by Van der Hammen and Wijmstra (1971) are shown besides the lithologic column. Facies interpretation, see Discussion.

EM3 makes up the largest fraction of the sediment followed by EM2 (Fig. 8). The composition of the sediments associated with the aeolian part of the Beuningen complex is different: EM3 and EM4 are virtually absent and EM2 dominates (Fig. 8). The upper part of unit OCII (29–30 m) shows a decrease in EM3 and EM4 and an increase in EM2 and EM1 compared to the interval below it.

The proportion of EM4 increases from a height of 30 m upwards and shows a peak in abundance in unit LLB (Fig. 8; more detail in Appendix C). It decreases sharply in unit YCI (which is typified by a mixture of EM1, EM2 and EM3) and increases again sharply in unit USL (Appendix C). The proportion of EM4 in unit USL is lower than in unit LLB. The pollen section corresponding to US and the lowermost part of YCII (Appendix D) displays a clear zonation: pollen zone 2a shows the characteristic high *Betula* count of the early Allerød and a high *Salix* count, zone 2 b has the characteristic high *Pinus* count of the later Allerød and zone 3 heralds the onset of the Younger Dryas, indicated by a decrease in *Pinus* and increase in herbs and grasses (*Poaceae*, *Ericales* and *Empetrum*).

Unit YCII is characterised by a strong predominance of EM2 and almost no contribution from EM3 and EM4 (Fig. 8). Unit DS is also strongly dominated by EM2, but in contrast to unit YCII the proportion of EM3 and EM4 is significant.

4.5. Temporal evolution in end-member and vegetation composition at Leusden

Unit OCII at the base of sediment profile M251 is characterised by a mixture of end members which is dominated by EM3 (Fig. 9). The concentration of loam laminae at approximately 2 m is marked by a higher proportion of EM4.

Unit LLB is strongly dominated by EM4 at the base, followed by an increase in EM3. The entire LLB is marked by high values of *Selaginella selaginoides*, a moss-like perennial forming a short dense vegetation (Fig. 10). *Poaceae* are relatively abundant, pointing to grassy upland plains. The arboreal pollen is dominated by *Pinus* (probably long-distance transport), but more local *Betula* is also present. In tandem with the transition from predominance of EM4 to EM3, the pollen composition changes slightly: *Hippophae* (possibly indicating bare sand patches), *Juniperus* (e.g. bordering *Betula* stands), *Dryas*, *Chenopodiaceae* and marsh herbs (*Cyperaceae* and *Potentilla* type) increase and *Selaginella selaginoides*, a poor competitor, decreases (Fig. 10).

Higher up in sediment profile M251, Unit YCI is initially marked by a mixture of all four end members (Fig. 9). This transitional zone in the end-member composition corresponds to local pollen zones L2 and L3 (Fig. 10). L2 is characterised by an increase both in *Betula* and *Juniperus*, and in *Poaceae* and *Scabiosa*, indicating a slightly denser arboreal and herb vegetation. Also, *Cyperaceae* and the aquatic *Sparganium* type increase, pointing to a denser wetland herb vegetation than before. In contrast to L1, *Selaginella selaginoides* is not present. The pollen composition of L3 shows a more open vegetation than that of L2: *Betula* (and the ratio of arboreal pollen to non-arboreal pollen) decreases significantly and several upland herbs of bare, open sunny patches increase (*Helianthemum*, *Tragopogon*, *Artemisia*, *Plantago maritima*, *Plumbaginaceae*) whereas *Poaceae* and *Cyperaceae* decrease markedly, also pointing to a thinner vegetation cover.

At sediment profiles DT1 and Lutterzand this transitional zone at the base of YC1 is not present and an abrupt transition to coarser end-members is observed. This composition is distinct from the preceding sandy-aeolian units due to the near absence of EM3 and EM4.

Pollen sections M222 and M241 show similar changes in pollen composition over time: In addition to the characteristic high *Betula* count, zone 2a is characterised by *Juniperus* and *Poaceae* (decreasing towards the top), and *Artemisia*, *Helianthemum* and marsh herbs (Fig. 10). Zone 2a thus shows a varied vegetation of trees/shrubs and upland and wetland herbs, together capable of trapping fine aeolian sediment. Zone 2 b is characterised by a decrease in the (mainly upland) herbs and grasses besides the characteristic double *Pinus* peak (Fig. 10; Hoek, 1997 A). Zone 2 b thus reflects both an increase of *Pinus* (probably at the higher, drier locations) and a strong relative decrease of the upland herb vegetation. There is a clear correlation between the sediment characteristics of profile M251 and the pollen composition of section M241: the EM4 dominated lower zone corresponds to pollen zone 2a and the EM3 dominated upper zone corresponds to pollen zone 2 b (Fig. 10). Sediment profile M5 and pollen section M222 (approximately 50 m apart) show a slightly different relationship between pollen and end-members: the EM3 dominance starts later in zone 2 b.

Similar to unit YCI, a transitional layer is observed at the base of unit YCII (M251 and M5; Fig. 9). The layer is not present at sediment profiles DT1 and Lutterzand. It is accompanied by a shift in the pollen composition from zone 2 b to zone 3 (Fig. 10). *Pinus* decreases and herbs and grasses increase (*Poaceae*, *Empetrum* and *Ericaceae*). *Betula* becomes the dominant tree (but decreases in abundance afterwards; zone 3 b of M222). The remainder of unit YCII shows a slightly more mixed ratio of the end-members than unit YCI: EM2 dominates and EM4 is absent, but EM3 is present (Fig. 9).

5. Discussion

5.1. Interpretation of end-members

The combination of different transport media (water/air) and different transport modes (creep/reptation/saltation/suspension) complicates the interpretation of end members (Fig. 11). Although viscosity and density of water differ from those of air, similar sorting processes apply, and thus no clear distinction between the transport media can be made based on the shape of size-shape distributions alone. For example, the average end-member composition of the Mekkelhorst Member and the upper part of the Older Coversand II at Lutterzand are quite similar and dominated by coarse end-members EM1 and EM2 (Fig. 8). Sedimentary structures clearly indicate fluvial processes for the Mekkelhorst member and (dry) aeolian processes for the upper part of OCII. It should therefore be stressed that, although transport modes can be readily distinguished using end-member verification samples alongside the technique introduced by Van Hateren et al. (2020), the interpretation of sedimentary structures is required to identify the transport medium. Another possibility is (automated) determination of the degree of frosting of the sediment grains. In an aeolian environment, the degree of frosting is significantly higher than in a fluvial environment due to the stronger impacts between grains during transport. The degree of frosting can therefore indicate the length and intensity of aeolian processes experienced by the sediment, which is termed 'aeolization' (Mycielska-Dowgiało and Woronko, 2004).

EM1, the coarsest primary component observed in the current study with a mode at 370 μm , shows a constant grain regularity with increasing size (Fig. 6). This shape of the SSD is characteristic for bedload transport (Van Hateren et al., 2020). A comparison to

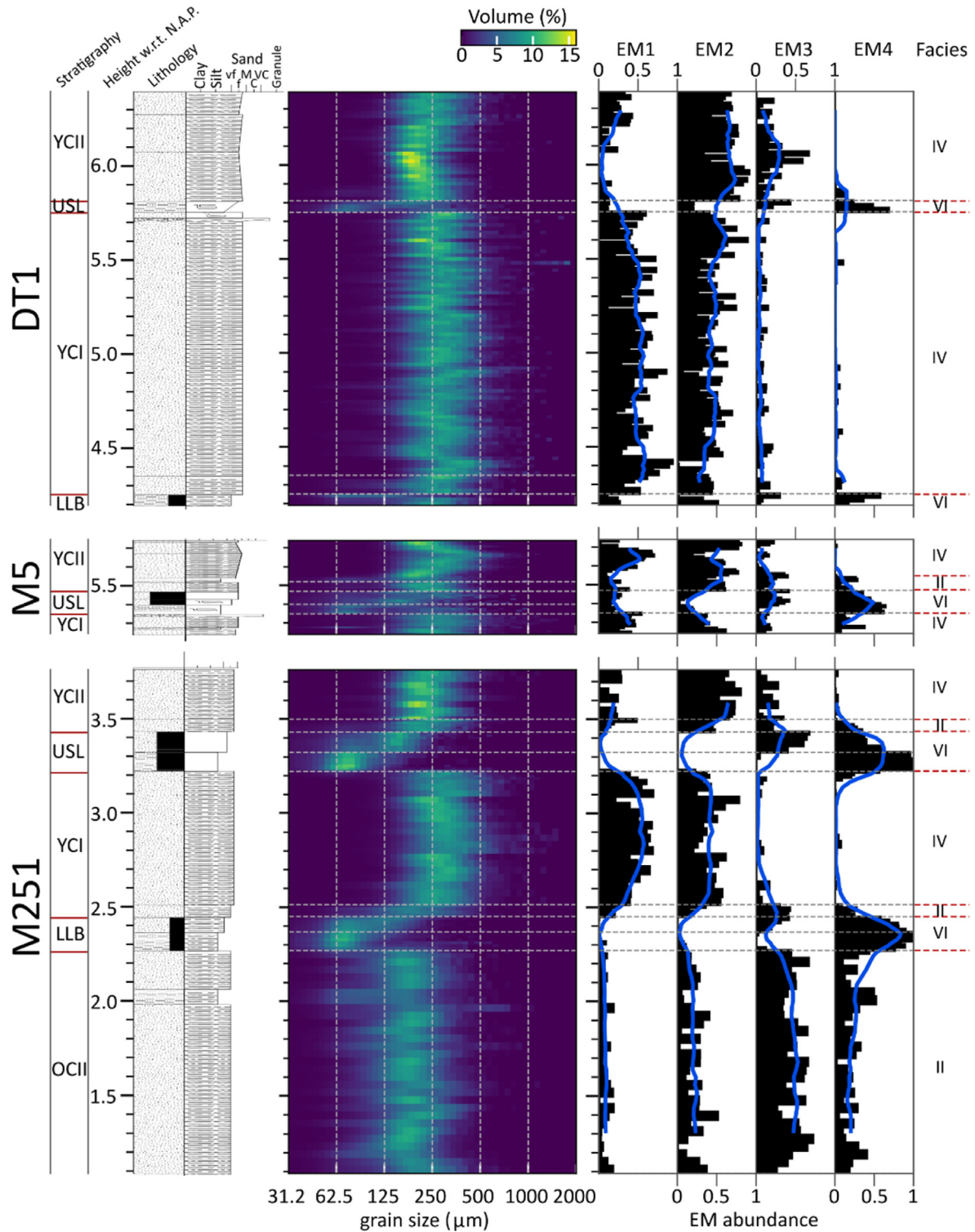
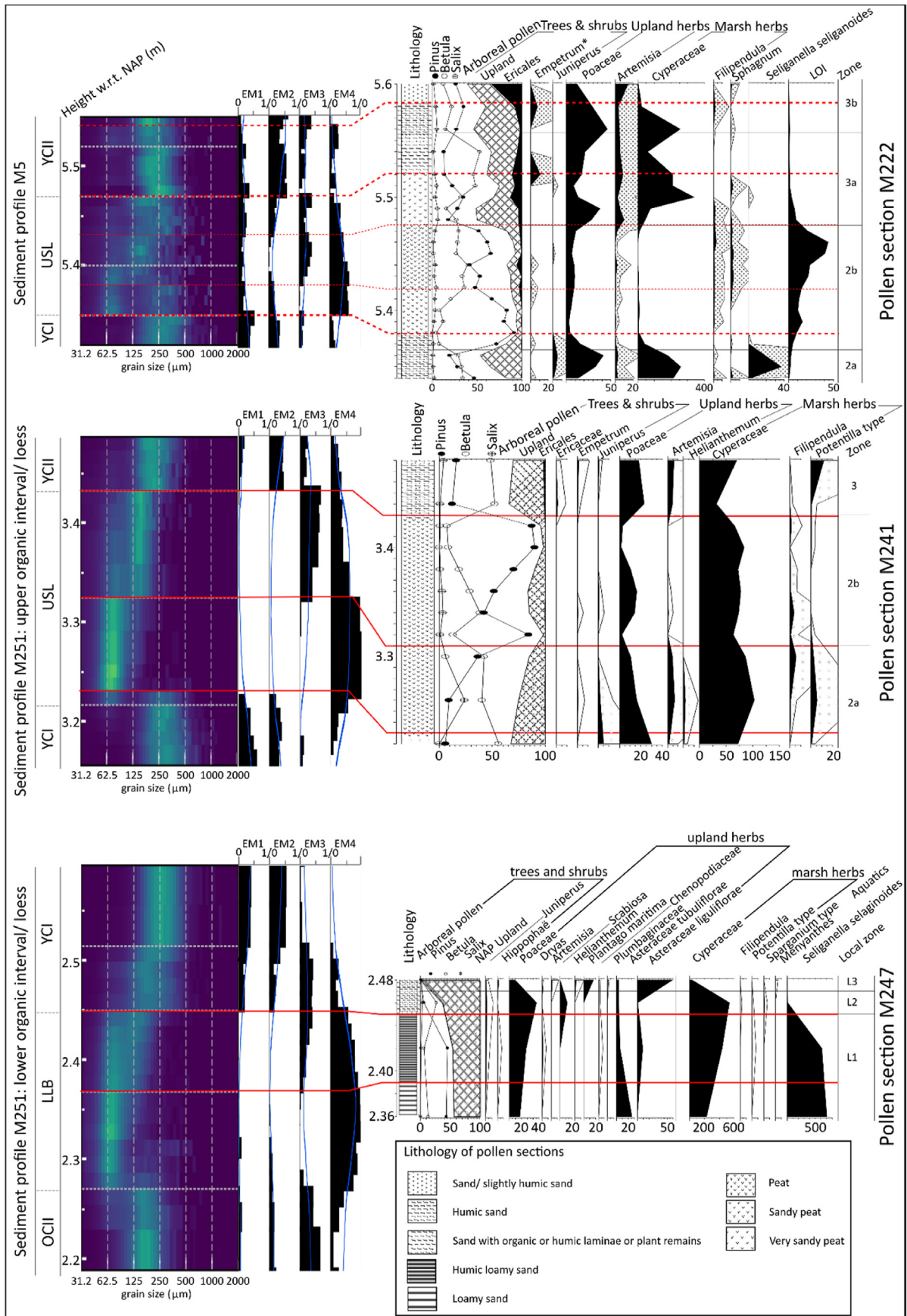


Fig. 9. End-member abundances for the Leusden sediment profiles with grain-size distributions and simplified lithologic columns for reference. Stratigraphic units as defined by Maarleveld and Van der Schans (1961) and Westerink (1981). The facies are discussed in the discussion chapter (5). Similar to unit LLB, unit USL displays a coarsening-upward trend marked by dominance of EM4 at the onset, followed by EM3 (Fig. 9). At sediment profile M251 the proportion of EM4 is significantly higher than at the other sites (100% at the onset; Fig. 9).

aeolian reference samples with known sedimentary structure shows that the end member is related to coarse bedload: it fits well to the coarser sand fraction of aeolian granule ripples (granule ripples form on a bed that is depleted in fines due to deflation) and low-angle cross bedding (dry aeolian deposit formed by wind

ripples on a sloping surface or low dune (Schwan, 1988)). The shape of the end member's size-shape distribution is also similar to that of the fluvial sediment from the Beuningen complex. However, the fluvial sediment is significantly coarser. In conclusion, the shape of the SSD and the relation to known sedimentary structures indicates



that it represents the coarse fraction of aeolian bedload (creep and reptation) (Fig. 11).

EM2, the second coarsest primary component with a mode at 220 μm , displays a very minor decrease in grain regularity with increasing size. Its size-shape signature is intermediate between EM1 and EM2 of Van Hateren et al. (2020). It therefore likely represents a fine-grained bedload component, mainly travelling in saltation, and slightly overlapping with modified saltation (hence the minor decline in grain regularity with increasing size; Van Hateren et al., 2020, Fig. 11). This interpretation corresponds with the correlation of the end member with the finer fraction of low-angle cross-bedded aeolian sediment (Fig. 7). The end member is very similar to the coarser fraction of adhesion ripples, consisting of grains creeping on a wet surface (Fig. 7; Fig. 6 in Kocurek and Fielder (1982)).

EM3 is finer-grained with a mode at 155 μm and shows a steeper decline in grain regularity compared to EM2. It likely represents modified saltation, i.e. the fraction of the saltating population that can be taken up into suspension by the wind and transported over a short distance, up to hundreds of metres (Van Hateren et al., 2020, Fig. 11). EM3 correlates to the finer fraction of adhesion ripple lamination, which indicates that it may be transported as modified saltation load and adhere to the adhesion ripples on a wet depositional surface (Fig. 7; fine fraction of Fig. 6 in Kocurek and Fielder (1982)). No other reference sample showed a good fit to the end member. In future work, more reference samples are required for a better understanding of the sedimentary processes associated with this end member.

EM4 shows a clear suspension signature, with a modal grain size of 71 μm , a regularly shaped silt fraction, and a coarser-grained tail consisting of highly irregular very fine to fine sand (Van Hateren et al., 2020). Since bedload transport is not possible in damp conditions, the correlation of EM4 to the lithogenic fraction in a peat underpins the interpretation as (sandy) loess (Fig. 7; Fig. 11).

However, the coarse sandy tail of EM4 is atypical of primary loess. This is probably an artefact from insufficient unmixing: the loams/loamy peats generally contain sand laminae consisting of modified saltation deposits that originate from nearby areas (Appendix E). Sand grains of the sand laminae are always present in the samples, and therefore cannot be entirely unmixed from the loess end member by end-member modelling (similar to a highly mixed dataset in the sense of Van Hateren et al., 2018).

5.2. Sedimentary facies and end-member composition

Facies I is bedload dominated with approximately equal proportions of EM1 and EM2 (Fig. 12). This end-member composition occurs at the base of the Lutterzand sediment profile and is associated with fining-up sequences that can be interpreted as shallow channel fills of a braided system (Van Huissteden et al., 2000, Fig. 8). The large proportion of modified saltation in the top of the fining-up sequences (EM3) may have a fluvial origin (short-term suspension from nearby channels) or may represent aeolian processes acting during base flow conditions in the dry summer months (Mountney and Russell, 2009; Good and Bryant, 1985; Kasse, 2002; facies 1). We therefore interpret the depositional environment to be a braided river plain (Fig. 12).

Facies II is dominated by fine saltation and modified saltation (EM2 and EM3), but all end-members are present in proportions that vary from sample to sample (Figs. 12, Fig. 8, Fig. 9). This end-

member composition occurs predominantly in unit OCI and the base of unit OCII at the sediment profile of Lutterzand, and throughout unit OCII in the sediment profile M251 of site Leusden. We propose that the associated depositional environment is a “wet” sand sheet: a nearly flat or sloping aeolian sand sheet that is receptive to (seasonally) varying surface humidity, causing alternations between dry aeolian bedload transport (mainly EM2 and EM1) and adherence of mainly modified saltation (EM3) but also suspended load (EM4) to a wet depositional surface (Fig. 12) (Schwan, 1986, facies 3; Kasse, 2002, facies 2). At site Lutterzand clay pebbles and flat channel structures indicate that shallow channels drain the sand-sheet surface during heavy rainfall or snowmelt, possibly related to an impermeable subsoil due to permafrost or deep seasonal frost (Bayard et al., 2005, Fig. 12). The abundance of adhesion ripples in unit OCII observed by Van Huissteden et al. (2001) is typical for a humid aeolian environment. This supports the association of facies II with a wet sand sheet.

Two dry aeolian facies are distinguished. Facies III is dominated by bedload (EM1 and EM2) with still a high amount of modified saltation (EM3) but little suspension (EM4) (Fig. 12). It shows a similar end-member composition to facies I, owing to the fact that both environments are bedload dominated, although having a different transport medium (Fig. 12). The sediments lack the (fluvial) fining-up sequences observed in facies I. Similar to facies II, bedding is predominantly horizontal (sand sheet). However, the decrease in the amount of modified saltation and suspension compared to facies II indicates drier bed conditions that largely preclude adherence of fine grains to the depositional surface (Schwan, 1986, facies 2; Kasse, 2002, facies 3). We therefore associate facies III with a “dry” aeolian sand sheet (Fig. 12). The facies only occurs in the upper part of the OCII unit of sediment profile Lutterzand (Fig. 8).

The other dry aeolian facies, facies IV is characterised by a very high bedload proportion, strongly dominated by EM2 and EM1, with a relatively low amount of EM3 (Fig. 12). Such a strong dominance of bedload can be best explained by lateral sorting in incipient dunes or undulations (Fig. 12) (Kasse, 2002, facies 3). In such an environment, different types of sediment may be deposited *simultaneously* at different places: coarse material is left behind in blowouts, fine bedload (EM2) is transported and deposited in undulations or incipient dunes (main sediment body) and grains susceptible to be taken up into suspension (EM3 and EM4) are only deposited under sufficiently quiescent conditions in relatively wet, low lying and potentially vegetated interdune areas or outside the dune fields. This leads to sediment deposits that are highly sorted in a vertical profile, but spatially heterogeneous (Van Hateren et al., 2020). This contrasts with the sand-sheet environment (facies II/facies III), where conditions are relatively similar over large distances. In such a spatially homogeneous environment, sediment sorting depends on variations in wind speed and/or surface humidity *through time*, leading to a deposit characterised by more variation in a vertical sediment profile. Both at Leusden and at Lutterzand, facies IV is associated with the Younger Coversand units. Although we generally observe horizontal bedding in these units, the inference of undulations or incipient dunes is corroborated by a dome-shaped dune structure near sediment profile M251 and low-angle cross-bedding (Kasse, 2002 and references therein). In addition, the lateral differences in soil development of the Usselo Soil (peat versus bleached soil) indicate the formation of

Fig. 10. End-member composition and pollen counts for site Leusden. Grain size distributions are shown for reference. The pollen sections M247 and M241 were obtained from the location of sediment profile M251. Red lines show the stratigraphic correlation. Pollen section M222 is located near M5, at approximately 50 m distance. The stratigraphic correlation is therefore not certain (dotted lines). (For interpretation of the references to colour in this figure legend, the reader is referred to the Web version of this article.)

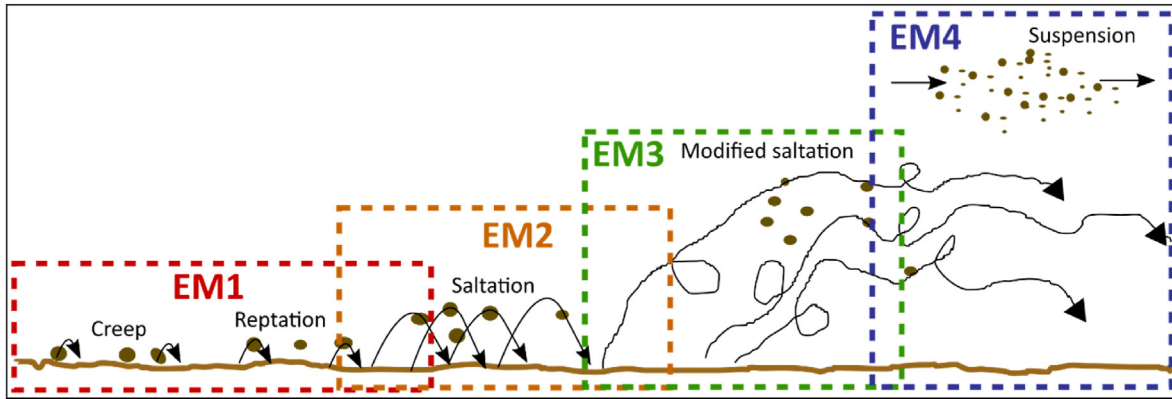


Fig. 11. Transport modes in water or air and associated end members.

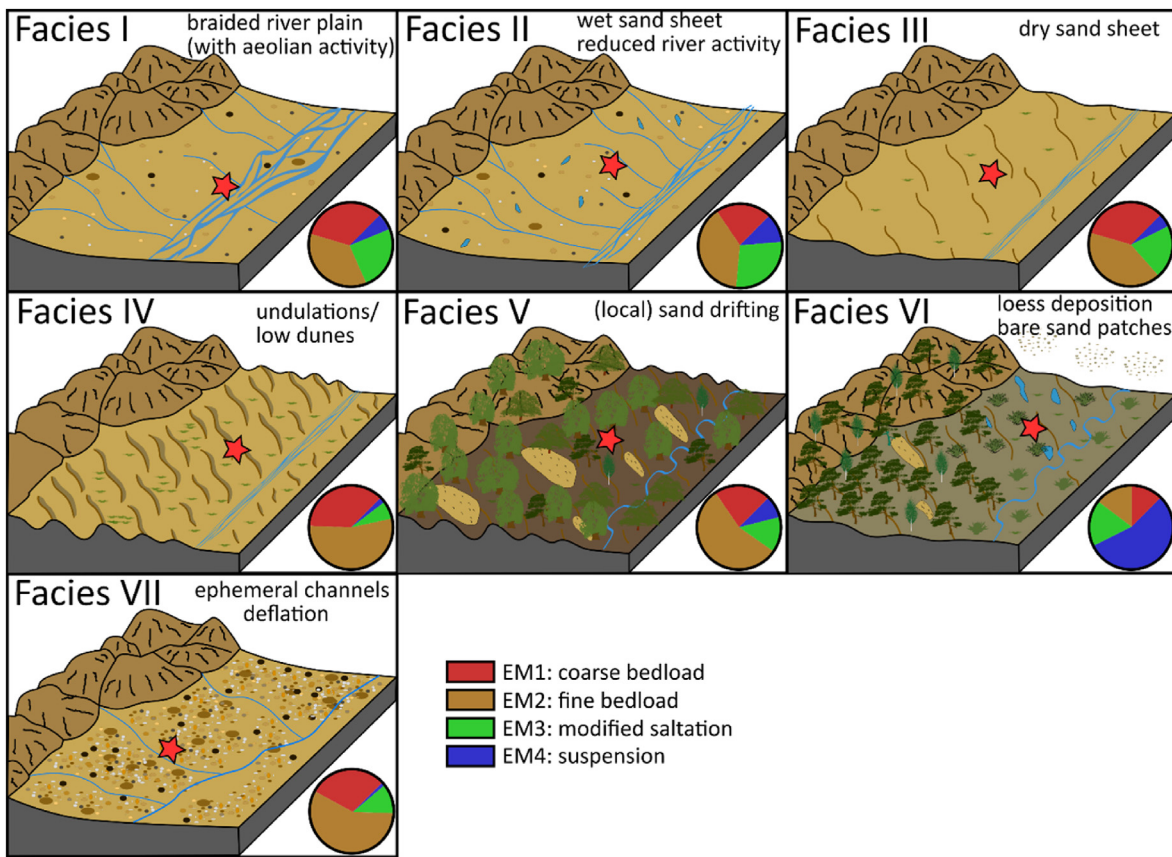


Fig. 12. Proposed depositional environments for the facies. Hills represent an ice-pushed ridge. Red stars mark where the facies is being formed. Pie-charts show the end-member composition that characterises the facies. The end-member composition of facies VII is only based on the aeolian bedload deposits and does not comprise the shallow fluvial channels nor the deflation horizons. River morphology after [Woolderink et al. \(2019\)](#) except for facies VII. (For interpretation of the references to colour in this figure legend, the reader is referred to the Web version of this article.)

low-dune relief during deposition of Younger Coversand I.

Facies V is associated with Drift Sand (unit DS) in the Lutterzand sediment profile and is not observed at Leusden. Similar to facies IV it is dominated by EM2 (Fig. 12). However, the proportion of EM1 is lower and the proportions of EM3 and EM4 are higher (Fig. 12). The drift sands were deposited in steep-sided dunes that developed in barren patches of sand within a generally vegetated landscape (e.g. [Vandenberghe et al., 2013, Fig. 12](#)). The denser vegetation cover of the Holocene may explain the decrease in EM1 (less transport energy due to small fetch length on the sandy patches) and increase in

EM3 and EM4 (trapping by vegetation and lower wind speed) compared to the other low-dune facies (IV). The loess and fine sand may derive from reworking of the USL and/or LLB unit.

Facies VI is markedly different from the previously discussed facies due to the predominance of suspended material (EM4). Suspension and modified saltation together make up approximately three quarters of the end-member composition (Fig. 12). The large proportion of suspension load indicates loess deposition as sediment dominated by silt indicates conditions favourable to the deposition of suspended material. Such favourable

environmental conditions are for example low wind speeds (climate or vegetation), obstruction of bedload (vegetation) or a wet/damp depositional surface (Fig. 12).

Facies VII is only associated with the Beuningen Complex (unit BC) in the Lutterzand sediment profile (Fig. 8). The facies is distinguished based on field observations and a size-shape distribution from the fluvial part of the Beuningen complex. It consists of a fluvial and aeolian component. The fluvial component is composed of coarse cross-bedded sand and gravel preserved in shallow channel structures. The size-shape distribution shown in Appendix F has a distinct bedload signature with coarse grain size and no trend in grain shape with increasing grain size. The channels have a restricted depth (~30 cm) and likely represent very shallow ephemeral channels. This is supported by the bimodal grain-size distribution of the sediment that may indicate waxing and waning flow conditions (Appendix F).

The thin gravel beds of the aeolian component of facies VII mark desert pavements composed of the sediment fraction incompatible with aeolian transport (Kasse et al., 2007). The processes of aeolian deflation and supply by ephemeral channels can occur simultaneously in a polar desert environment due to the long periods of drought interspersed with snowmelt (Fig. 12; Rains et al., 1980; Kasse et al., 2007). The aeolian lag deposit generally occurs on top because it develops after prolonged inactivity of ephemeral channels in a specific area (Rains et al., 1980). Bedload-dominated aeolian sand occurs in between the lag deposits. The shift from EM1 at the base to EM2 at the top may represent a gradual decrease in transport energy, marking the transition from the deflation dominated Beuningen unit to the quick aggradation observed in unit OCII (Vandenberghe et al., 2013).

5.3. Landscape evolution and forcing mechanisms

The shift of the Mekkelhorst Member to unit OCI at Lutterzand occurred at or before approximately 23.3 ± 1.8 ka (the oldest age of the facies II deposits in profile 4 of Vandenberghe et al., 2013). The shift from a braided river plain (facies I) to a wet sand sheet (facies II) marks the onset of sandy aeolian deposition and may indicate climate-driven aridification or a system intrinsic change (e.g. change of the river position). The climatic and system-intrinsic factors cannot be differentiated because no sediments from this time frame were studied at Leusden to allow for a comparison. However, climatic aridification fits with observations from the southern Netherlands (shift from fluvial to fluvio-aeolian deposition; Kasse et al., 2007), central Germany (transition from braided river floodplain to loess accumulation; Lauer et al., 2014), Belgium and Normandy (France) (increase in sedimentation rate of loess; Van Vliet-Lanoë, 1989), and Poland (gradual transition from braided river to aeolian deposition; Bohncke et al., 1995). A tentative link can be made with the significant warming around 23 ka in ice-core records from Greenland (Kindler et al., 2014). Increased evaporation due to warming and low precipitation due to the continental climate may have caused the aridification.

Facies VII deposits (polar desert environment) of the Beuningen Complex are dated to 23.5 ± 1.8 ka – 16.1 ± 1.3 ka at Lutterzand (Vandenberghe et al., 2013). The widespread occurrence of deflation horizons (Beuningen Gravel Bed; Kasse et al., 2007) and the low average deposition rate (Vandenberghe et al., 2013) indicate a low ratio of deposition to erosion. A high amount of erosion can be attributed to constant reworking of aeolian sediment by intermittent flow in channels like in present day deserts and an enhanced pressure gradient over northwest Europe during the Late Pleniglacial which caused increased wind speed during this period, enhancing the available transport energy for aeolian processes (Renssen et al., 2007). A low amount of deposition can be attributed

to deep seasonal frost, limiting the depth of reworking and therefore the availability of sediment and a decrease in fluvial activity. Due to fluvio-thermal erosion, fluvial processes entrain more sediment from a frozen soil than aeolian processes (Fuchs et al., 2020). Sediment availability is therefore reduced by a decrease in fluvial activity.

The Older Coversand II (Unit OCII) represents high deposition rates during the final Late Pleniglacial, prior to the Bølling biochronozone (Vandenberghe et al., 2013). We attribute the high deposition rates to three causes: 1) An increase in humidity: facies II reflects an intermittently wet (EM3 and EM4) and dry (EM1 and EM2) depositional surface, which is in stark contrast to the preceding polar desert phase and may be linked to a northward shift of the polar front that preceded the Bølling warming (Cowling et al., 2020). 2) A decrease in wind speed, also linked to the northward shift of the polar front. 3) Disappearance of permafrost from the upper layers of sediment (Kasse, 1997; Van Huissteden et al., 2000), increasing the availability of loose, erodible sediment.

At Lutterzand, a shift within unit OCII from facies II to III indicates drying of the environment (wet to dry sand-sheet environment) (Fig. 8). This trend is absent at Leusden site M251 (Fig. 9). This dissimilarity indicates a system-intrinsic/local explanation for the presence or absence of the drying trend: at Lutterzand, the accumulation of highly permeable aeolian sediment above the groundwater table (undulation or low dune) leads to a shift from a humid to a dry sand-sheet environment (Table 2). This system-intrinsic mechanism is precluded at Leusden site M251 due to groundwater seepage from the sandy aeolian plateau and ice-pushed ridge, caused by the paleo-topographic position on the slope from the sandy aeolian plateau to the Amersfoort glacial basin (Fig. 2; Table 2).

We propose that the onset of the Bølling interstadial in sediment profiles M251 (Leusden) and Lutterzand is marked by the wavy/crinkly lamination with loam bands in the upper part of OCII (alternation of facies II/III and facies VI; Fig. 8; Fig. 9). The intermittent deposition of loam bands (facies VI) supports a vegetated surface or a (seasonally/episodically) wet surface on which

Table 2

Comparison of the temporal trend in facies at the studied sediment profiles (summary of Figs. 8 and 9). The subdivision into relatively dry and relatively wet sites is based on the facies difference of the upper part of unit OCII and peat formation in unit LLB (DT1, M251) and unit USL (M251, M5). The transition rows denote the transitional facies between two units (left empty if not present). The facies distinguished by Kasse (2002) are shown for reference and are denoted by arabic rather than roman numerals. Kasse (2002) described the facies as follows: Facies 1 consists of massive or indistinct horizontal bedding, interpreted as aeolian deposits reworked by intermittent fluvial activity (shallow channels) and strongly affected by cryogenic processes (fluvio-aeolian deposits). Facies 2 comprises alternating bedding of fine sandy and silty fine sandy aeolian deposits, respectively laid down during dry and/or stronger wind conditions and wet and/or weak-wind conditions. Facies 3 encompasses horizontally laminated to low-angle cross-bedded fine sandy aeolian deposits, deposited in the form of small wind ripples or planar beds on a dry surface. Facies 4 involves large-scale dune slipface cross-bedding in sandy aeolian deposits (rare in deposits in the Netherlands, more common in Poland).

Stratigraphic unit	Relatively dry (high) locations		Relatively humid (low) locations		Kasse (2002) Generalised
	Lutterzand	DT1	M251	M5	
DS	V	–	–	–	3 (2,4)
YCII	IV	IV	IV	IV	3 (2,4)
Transition			II	II	–
USL	VI	VI	VI	VI	–
YCI	IV	IV	IV	IV	3
Transition			II	–	–
LLB	VI	VI	VI	–	3
OCII (upper)	III	–	II	–	3
OCII (lower)	II	–	–	–	2/3

suspended load can be trapped (Schwan, 1986). The continuation of bedload transport (facies III) favours the wet surface hypothesis, as it indicates an open landscape, which signals a lag in the response of vegetation to the wetter (and warmer) interstadial conditions.

At the base of the LLB unit, the shift from sand-sheet to loess deposition is likely the result of a positive feedback cycle leading to a closing of the landscape by vegetation: the humid conditions of the Bølling favour deposition and adhesion of loess to the surface, decreasing infiltration capacity and enhancing humidity and stability of the sediment bed. The stable conditions aid colonisation of the former barren sand sheet by vegetation, which in turn traps more loess and impedes bedload transport. Humid conditions are corroborated by the high values of *Selaginella selaginoides*, a perennial vascular plant that thrives in humid conditions (like base-rich fens, wet upland grasslands, dune slacks) and by *Cyperaceae* that likely occupied the wetter positions in the landscape (Fig. 10). The perennial and evergreen *Selaginella selaginoides* (earlier part of the Bølling) likely formed a thick moss-like carpet year-round that is very effective in trapping loess and decreasing bedload transport. In the upland (drier) parts of the landscape, plant groups such as the *Asteraceae tubiflorae* contributed to the trapping of loess (by decreasing the near-surface wind speed) and obstruction of bedload transport.

The onset of the deposition of the Younger Coversand I unit during the Older Dryas is expressed differently in sediment profile M251 (Leusden) than in profiles Lutterzand and DT1 (Leusden). M251 displays a transition from loess (facies VI) via wet aeolian facies II to dry aeolian facies IV. The transition zone belongs to the Older Dryas biochronozone (pollen zones L2 and L3) (Fig. 10). No transitional zone is present at sediment profiles DT1 and Lutterzand (Table 2). This contrast, and the formation of peat at sediment profile M251, suggests that the sediment bed was relatively humid at sediment profile M251, and relatively dry at sediment profiles DT1 and Lutterzand (Table 2). During the transition from the Bølling to the Older Dryas, the relatively dry locations are more sensitive to disturbance of vegetation and to aeolian action. Bedload transport is therefore initiated earlier in the Older Dryas. The modified saltation fraction that originates from these open patches travels on the order of a few hundred meters (Van Hateren et al., 2020) and is trapped at more humid locations such as sediment profile M251 by sustaining patches of vegetation consisting of grass, *Betula* (likely partly *Betula nana*) and herbs such as the rather tall perennial herb *Scabiosa*. This explains the large proportion of modified saltation observed in the transitional zone of sediment profile M251.

The overlying facies IV deposits of unit YCI mark a return to an open landscape and bedload dominated sandy aeolian deposition. However, the end-member composition is distinctly different from the preceding sand-sheet units and indicates deposition in undulations or incipient dunes. Formation of undulations or incipient dunes may be explained by remnant patchy herbaceous vegetation that traps bedload on its lee side, inducing incipient dunes and thereby swiftly transforming a sand-sheet environment to an incipient dune field (similar to the effect of *Calamagrostis arenaria* (marram grass) on a beach plain).

The herbaceous vegetation at Leusden consists initially of *Plantago maritima*, *Asteraceae liguliflorae*, *Artemisia* and *Helianthemum* (Fig. 10: pollenzone L3). Van Geel et al. (1989) describe the vegetation of the Older Dryas at a locality approximately 20 km southwest of the Lutterzand sediment profile: a herbaceous pollen composition consisting of *Artemisia*, *Helianthemum*, *Plantago*, *Rumex*, *Thalictrum*, *Selaginella selaginoides*, *Asteraceae tubuliflorae*, *Potentilla type and Sanguisorba officinalis*. Large slip-face dunes are rare in this period (Kasse, 2002), possibly because the small and patchy herbaceous vegetation has insufficient capacity to keep up with the sedimentation.

In the Usselo Soil and the peat deposits of Allerød age (USL unit) a return to loess deposition of facies VI is recorded (Table 2). Climate change is the likely driver of the facies shift, underpinned by the similarity in the change in sedimentary environment shown by the sediment profiles (Fig. 8; Fig. 9). All sediment profiles display a more abrupt increase in suspended load compared to the LLB unit. This may indicate a more rapid occupation by vegetation, possibly because the remnant herbal vegetation of the Older Dryas allowed a quicker colonisation of the sand surfaces (unit YCI). This inference is corroborated by the pollen diagrams, which display a much more abrupt increase of especially *Betula* compared to the Bølling (Fig. 10: pollen zone 2a).

Because pollen- and sedimentological sampling was carried out at relatively high resolution at site M251 (Fig. 10), we can discuss the relationship between the response of the aeolian system and vegetation in detail. Contrary to the expected relationship between vegetation density, associated surface roughness and loess proportion, the initial domination by loess (EM4) corresponds to the less dense *Betula* and herb-dominated vegetation of pollen zone 2a, whereas the modified saltation (EM3) dominated zone corresponds to the more mature and dense *Pinus* phase of the Allerød. This temporal trend may be explained by 1) a decrease in the availability of loess (EM4): during the early stage, unvegetated areas where still producing dust (river plains and chipping of sand grains during aeolian bedload transport). The subsequent widespread landscape stabilisation by pine woodlands must have led to a decline in the areal extent of dust sources. 2) An increase in the amount of modified saltation (EM3): pine woodlands are characterised by higher evapotranspiration rate and rainfall inception compared to herbaceous vegetation (Rannik et al., 2002; Batelaan and De Smedt, 2007) and therefore may induce a lowering of the groundwater table. They are furthermore highly susceptible to wildfire (Tanskanen et al., 2005) and the abundance of charcoal in the Usselo soil (also at DT1) confirms the occurrence of woodland fires during the Allerød (Van der Hammen and Van Geel, 2008). The drier bed conditions and occasional woodland fires may cause localised bedload transport on open patches, delivering sand by modified saltation to proximal downwind areas.

Similar to the base of the YCI unit, the base of the YCII unit (Younger Dryas, pollen zone 3; Fig. 10) indicates the effect of local conditions: sand-humic sand duplets occur at relatively humid locations (sediment profiles M251 and M5), whereas an abrupt transition to facies IV deposition occurs at the relatively dry locations (DT1 and Lutterzand) (Table 2).

The facies IV deposits of unit YCII mark a return to an open landscape and bedload dominated sandy aeolian deposition in undulations or incipient dunes similar to the environment associated with the YCI. At Lutterzand, the YCII unit almost completely lacks EM3 and EM4. This indicates a relatively open sandy aeolian plain with sparse vegetation that initiates incipient dunes, but has insufficient density to trap modified saltation. In contrast, the YCII unit of the Leusden sediment profiles shows a modified saltation component (EM3). The admixture is both present at the relatively dry/high location DT1 and the relatively humid/low locations represented by M5 and M251 (Table 2). The modified saltation component (EM3) therefore does not reflect more humid conditions, but rather an increased vegetation density in the Younger Dryas compared to the Older Dryas: Van Geel et al. (1989) describe a herbaceous pollen composition for the Older Dryas near Lutterzand. For the Younger Dryas, Hoek (1997 B) describes a dwarf shrub tundra intermingled with herbaceous vegetation for the northern Netherlands, and even a patchwork with tree stands for the southern Netherlands. The increased vegetation density also ties in with the sharper relief associated with the Younger Dryas dunes (observed at Lutterzand, Leusden and other localities; Westerink,

1981, Fig. 2; Maarleveld and Van der Schans, 1961; Van der Hammen and Wijmstra, 1971; Pons and Wiggers, 1958). It is also corroborated by the contrast in pollen composition between the Older and Younger Dryas.

The sand-seas are largely stalled by the development of a dense vegetation cover during the Holocene, as evidenced by the occurrence of a podzol soil profile in the top of the YCII deposits. In sediment profile Lutterzand, facies V deposits on top of the podzol evidence re-initiation of sand drifting (Fig. 8). This is generally attributed to disturbance of the vegetation cover by human activity, lasting predominantly from ~1ka until recently (Vandenberghe et al., 2013 and references therein). Although the drift sand areas were quite extensive (Pierik et al., 2018), the end-member composition is characterised by a higher contribution of modified saltation (EM3) and suspension (EM4). This likely reflects the wetter climate during the Holocene compared to the Older and Younger Dryas (allowing the deposition of fines onto the sediment bed).

6. Conclusions

Our results show that end-member modelling on grain size-shape distributions helps to reconstruct past environmental changes. Four end-members are distinguished within the aeolian deposits at Lutterzand and Leusden. Based on their characteristic size-shape distributions and comparison to reference samples, these end-members represent:

- End member 1: the coarse fraction of aeolian bedload (creep and reptation) or fluvial bedload. This interpretation is corroborated by the resemblance of the end-member to the coarse sand fraction of aeolian granule ripples and aeolian low-angle cross-bedding.
- End member 2: the fine fraction of aeolian bedload (saltating population). This ties in with the fact that its size-shape distribution resembles the fine fraction of aeolian low-angle cross-bedding.
- End member 3: modified saltation load (the fraction of a saltating population that is susceptible to short-term suspension). This end member is mainly associated with aeolian deposition in a humid sand-sheet environment or in front of an approaching dunefield or dry aeolian sand sheet. This interpretation is corroborated by the resemblance to the fine fraction of adhesion ripple lamination.
- End member 4: suspension load (loess). The interpretation is validated by the resemblance of this end-member to the lithogenic fraction found in peat (where bedload transport is not possible).

Although transport modes can be readily distinguished using end-member modelling of size-shape distributions, the interpretation of sedimentary structures is required to identify the transport medium (water/air). Sedimentary facies are reconstructed based on distinct mixtures of the four end-members and sedimentary structures. These facies reflect the sedimentary environment and therefore enable landscape reconstruction.

Synchronous changes in sedimentary environment at Lutterzand and Leusden indicate Late Pleniglacial to Late Glacial climate change as external driver:

- During the final Late Pleniglacial and early Bølling (~15.2 ± 1.2 ka until early Greenland Interstadial 1e), a wet sand-sheet environment prevailed (Older Coversand II unit), characterised by alternating deposition of bedload, modified saltation and suspension load (facies II). The facies shift from the preceding polar

desert environment of the Beuningen Complex (23.5 ± 1.8 ka – 16.1 ± 1.3 ka) indicates increased humidity and decreased wind speed. The onset of wet sand-sheet deposition may be linked to a northward shift of the polar front preceding the Bølling warming. The persistence of wet-sand sheet deposition into the Bølling indicates a gradual response of the sedimentary environment to the abrupt climatic event.

- The Lower Loamy Bed (Bølling/Greenland Interstadial 1e) is characterised by a marked increase in the deposition of suspended load (loess). This reflects humid conditions, the presence of a locally dense vegetation cover and potentially a decrease in wind speed. Pollen analysis confirms the humid conditions and presence of vegetation.
- Dry aeolian deposition is renewed in the Older Dryas (Greenland Interstadial 1 d). Compared to the preceding sand-sheet deposits, the end-member composition is poorer in modified saltation and suspension, suggesting that sparse herbaceous vegetation persisted to initiate aeolian undulations and incipient dunes, allowing a higher degree of sediment sorting (facies IV).
- The onset of the Allerød interstadial (Greenland Interstadials 1a, 1 b and 1c) is marked by a sharp increase of suspended load (facies VI). The high fraction of suspended load indicates that the initial *Betula* phase was humid and that the landscape became more vegetated. A subsequent increase in modified saltation and decrease in suspended load indicates that the *Pinus* phase was drier with patches of open sand, potentially caused by (*Pinus*-induced) drought and wildfires.
- The Younger Dryas (Greenland Stadial 1) is characterised by aeolian bedload deposition in undulations, incipient dunes and dunes. The end-member composition is similar to that of the Younger Coversand I and likewise suggests locally enduring herbaceous/shrub vegetation that formed nuclei for dune growth. At Leusden, a minor increase in modified saltation compared to the Older Dryas indicates that the vegetation of the Younger Dryas is denser and that deposition is more localised.
- Human-induced sand-drifting in the Middle Ages also resulted in dune formation. The higher proportion of modified saltation and suspension compared to the Older and Younger Dryas reflects the wetter climate and denser vegetation (forest) of the Holocene.

However, we also observe differences in sedimentary facies development between the study sites, which reflect the contrast between relatively high and relatively low paleo-topographical positions:

- At intermediate or relatively high paleo-topographical positions, the accumulation of highly permeable aeolian bedload causes a lowering of the *relative* groundwater table and thus leads to a drying-up sequence. At relatively low-lying locations, groundwater is supplied from the surroundings, allowing the groundwater table to rise in tandem with sediment accumulation. The drying-up trend is therefore forestalled.
- The response of the aeolian system to colder and drier climate conditions is more gradual under local humid conditions: these allow a sustaining vegetation cover, which delays the transition to bedload-dominated conditions.

Role of the funding source

The research was funded by the Department of Earth Sciences at Vrije Universiteit Amsterdam. Funding was acquired by the Sediment Laboratory.

Author contributions

Hans van Hateren: conceptualization, methodology, software, validation, formal analysis, investigation, writing – original draft, writing – review and editing, visualization. Cornelis Kasse: conceptualization, investigation, writing – review and editing. John van der Woude: conceptualization, validation, investigation (pollen analysis), writing – review and editing, visualization. Jeroen Schokker: conceptualization, investigation, writing – review and editing. Maarten Arnoud Prins: conceptualization, methodology, investigation, writing – review and editing, supervision, project administration, funding acquisition. Ronald Theodorus van Balen: conceptualization, sampling, investigation, writing – review and editing, supervision, project administration.

Declaration of competing interest

The authors declare that they have no competing financial interests or personal relationships that could appear to influence the

work reported in this paper.

Acknowledgements

We want to express our gratitude to two anonymous reviewers, whose comments significantly improved our manuscript. We thank Martine Hagen of the Sediment Laboratory for support during the lab work. Furthermore we would like to express our gratitude to the research group led by professor Jos Bazelmans. The research that this group carried out on (the context of) Allerød pine forest remains at Leusden has made available several sediment profiles, has provided valuable insights and age information. We thank dr. Jacqueline van Leeuwen for help with determining specific pollen types. We thank Dr. Hessel Woolderink for help with the sampling at Lutterzand and Leusden.

Appendix

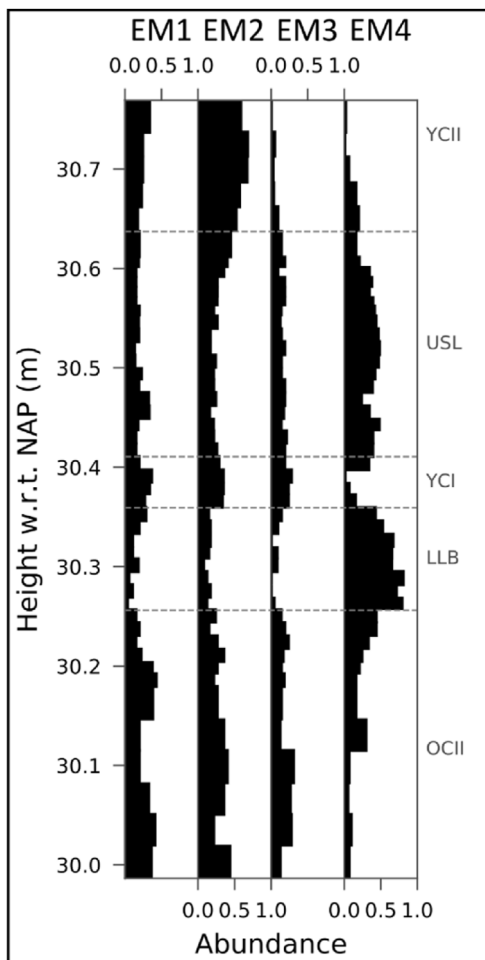


Appendix A. Additional sedimentary structures observed at site Leusden within the Younger Coversand I unit (YCI). A1: ice-wedge cast or large frost crack near sediment profile DT1 (between black arrows). A2: cross-bedded set of coarse sand and granules near sediment profile DT1. A3: dome-shaped dune structure near sediment profile M251.

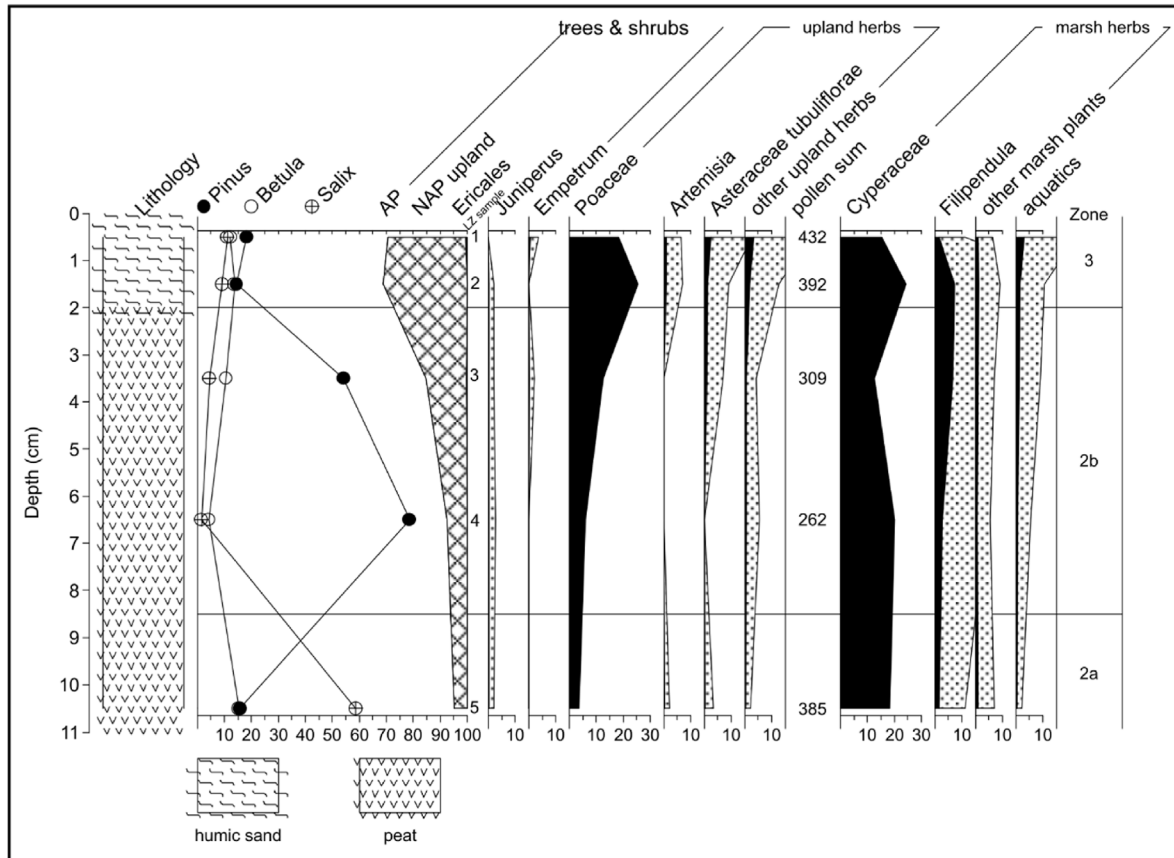
Appendix B

Correlation (R2) between end members and end-member verification samples. Adh. = adhesion. A colour scale was added to aid interpretation of the results. R2 values of this scale increase by 0.1 per colour and range from 0.5 to 0.9 in the order: blue, green, yellow, orange.

EM	Fluvial Beun.	Aeolian deflation	Granule ripple	Granule ripple	Low-angle X-bedding	Adh. ripple	Loess (below LLB)	Loess (LLB)	Loess (LLB)	Peat
1	0.38	0.06	0.61	0.53	0.59	0.14	0.00	0.00	0.01	0.01
2	0.16	0.28	0.61	0.62	0.73	0.79	0.02	0.02	0.02	0.03
3	0.05	0.38	0.26	0.36	0.38	0.71	0.02	0.05	0.05	0.20
4	0.01	0.38	0.02	0.04	0.03	0.09	0.52	0.63	0.83	0.54



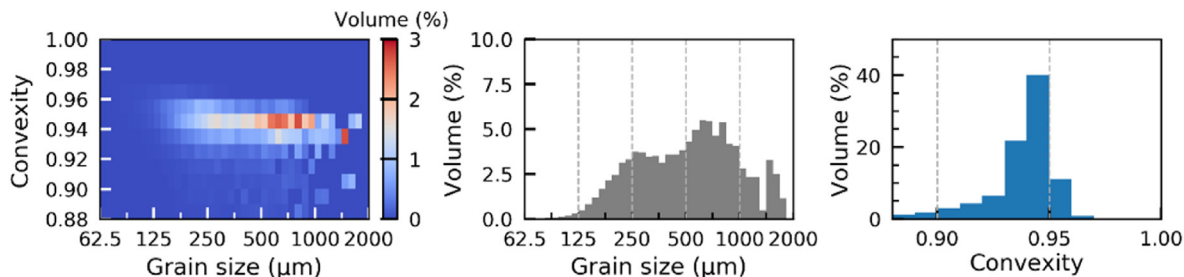
Appendix C. End-member proportions of the Lutterzand sediment profile for the interval consisting of units LLB, YCI and USL.



Appendix D. Pollen composition of pollen section Lutterzand (Allerød peat at the location of profile 1 of [Vandenberghe et al. \(2013\)](#)).



Appendix E. Close-up of the loamy peat (Allerød; lower part) and laminated sand-organics (Younger Dryas; upper part) of sediment profile M5 (photograph used with permission of the Cultural Heritage Agency of the Netherlands).



Appendix F. Grain size-shape distribution (left, volume as colour scale), grain size distribution (middle) and grain shape distribution (right) of the sediment in a shallow channel structure associated with the Beuningen Complex at site Lutterzand.

References

Batelaan, O., De Smedt, F., 2007. GIS-based recharge estimation by coupling surface–subsurface water balances. *J. Hydrol.* 337 (3–4), 337–355. <https://doi.org/10.1016/j.jhydrol.2007.02.001>.

Bateman, M.D., 1995. Thermoluminescence dating of the British coversand deposits. *Quat. Sci. Rev.* 14, 791–798. [https://doi.org/10.1016/0277-3791\(95\)00053-4](https://doi.org/10.1016/0277-3791(95)00053-4).

Bateman, M.D., 1998. The origin and age of coversand in north Lincolnshire, UK. *Permafrost. Periglac. Process.* 9, 313–325. [https://doi.org/10.1002/\(SICI\)1099-1530\(199810/12\)9:4<313::AID-PPP297>3.0.CO;2](https://doi.org/10.1002/(SICI)1099-1530(199810/12)9:4<313::AID-PPP297>3.0.CO;2).

Bayard, D., Stähli, M., Parriaux, A., Flüeler, H., 2005. The influence of seasonally frozen soil on the snowmelt runoff at two Alpine sites in southern Switzerland. *J. Hydrol.* 309 (1–4), 66–84. <https://doi.org/10.1016/j.jhydrol.2004.11.012>.

Bazelmans, J., Van Balen, R., Bos, J., Brinkkemper, O., Colenberg, J., Doeve, P., van Geel, B., Hakbijn, T., van Hateren, H., Hoek, W.Z., Huisman, H., Jansma, E., Kasse, C., van Os, B., van der Plicht, H., Schokker, J., Van der Putten, N., van der Woude, J., 2021. Environmental changes in the late Allerød and early Younger Dryas in The Netherlands: a multiproxy high-resolution record from a site with two *Pinus sylvestris* populations. *Quat. Sci. Rev.* 272. <https://doi.org/10.1016/j.quascirev.2021.107199>.

Beug, H.-J., 2015. *Leitfaden der Pollenbestimmung*. Verlag Dr. Friedrich Pfeil, München.

- Bohncke, S., Kasse, C., Vandenberghe, J., 1995. Climate induced environmental changes during the Vistulian Lateglacial at Żabinko, Poland. *Quaes. Geogr.* 4, 43–64. Special Issue.
- Bokhorst, M.P., Vandenberghe, J., Sümegi, P., Łanczont, M., Gerasimenko, N.P., Matviishina, Z.N., Markovic, S.B., Frechen, M., 2011. Atmospheric circulation patterns in central and eastern Europe during the Weichselian Pleniglacial inferred from loess grain-size records. *Quat. Int.* 234 (1–2), 62–74. <https://doi.org/10.1016/j.quaint.2010.07.018>.
- Cowling, O.C., Thomas, E.K., Svendsen, J.I., Mangerud, J., Vasskog, K., Hafliðason, H., 2020. Northward shifts in the polar front preceded Bølling and Holocene warming in southwestern Scandinavia. *Geophys. Res. Lett.* 47 (14), e2020GL088153. <https://doi.org/10.1029/2020GL088153>.
- De Moor, G., 1981. Periglacial deposits and sedimentary structures in the upper Pleistocene infilling of the Flemish Valley (NW Belgium). *Biul. Peryglac.* 28, 277–291.
- Drenova, A.N., Chikolini, N.I., Timireva, S.N., 1997. Late glacial dune-building in the Russian plain. *Quat. Int.* 41, 59–66. [https://doi.org/10.1016/S1040-6182\(96\)00037-7](https://doi.org/10.1016/S1040-6182(96)00037-7).
- European Environment Agency, 2020. March 13). <https://www.eea.europa.eu/data-and-maps/data/digital-elevation-model-of-europe>.
- Faegri, K., Iversen, J., 1989. In: Faegri, K., Kaland, P.E., Krzywinski, K. (Eds.), *Textbook of Pollen Analysis*. John Wiley and Sons, Chichester.
- Fuchs, M., Nitze, I., Strauss, J., Günther, F., Wetterich, S., Kizyakov, A., Fritz, M., Opel, T., Grigoriev, M.N., Georgy, T., Grosse, G., 2020. Rapid fluvio-thermal erosion of a yedoma permafrost cliff in the Lena River Delta. *Front. Earth Sci.* 8 (336). <https://doi.org/10.3389/feart.2020.00336>.
- Good, T.R., Bryant, I.D., 1985. Fluvio-aeolian sedimentation—an example from Banks Island, NWT, Canada. *Geogr. Ann. Phys. Geogr.* 67 (1–2), 33–46. <https://doi.org/10.1080/04353676.1985.11880128>.
- Grimm, E.C., 2004. *TILIA and TGView Software*. Illinois State Museum. Research and Collection Center.
- Hoek, W.Z., 1997. Late-glacial and early Holocene climatic events and chronology of vegetation development in The Netherlands. *A Veg. Hist. Archaeobotany* 6 (4), 197–213.
- Hoek, W.Z., 1997. *B. Palaeogeography of Lateglacial Vegetations; Aspects of Lateglacial and Early Holocene Vegetations, Abiotic Landscape, and Climate in The Netherlands*. ISBN 90-6809-250-2. Nederlandse Geografische Studies). ISBN 90-803900-1-1 (Thesis).
- Hoek, W.Z., Bohncke, S.J.P., 2001. Oxygen-isotope wiggle matching as a tool for synchronising ice-core and terrestrial records over Termination 1. *Quat. Sci. Rev.* 20 (11), 1251–1264. [https://doi.org/10.1016/S0277-3791\(00\)00150-5](https://doi.org/10.1016/S0277-3791(00)00150-5).
- Hunter, R.E., 1980. Quasi-planar adhesion stratification: an eolian structure formed in wet sand. *J. Sediment. Res.* 50 (1), 263–266. <https://doi.org/10.1306/212F79C8-2B24-11D7-8648000102C1865D>.
- Kalińska-Nartiša, E., Thiel, C., Nartišs, M., Buylaert, J.-P., Murray, A.S., 2016. The north-eastern aeolian 'European Sand Belt' as potential record of environmental changes: a case study from Eastern Latvia and Southern Estonia. *Aeolian Res.* 22, 59–72. <https://doi.org/10.1016/j.aeolia.2016.06.002>.
- Kasse, C., 2002. Sandy aeolian deposits and environments and their relation to climate during the Last Glacial Maximum and Lateglacial in northwest and central Europe. *Prog. Phys. Geogr.* 26 (4), 507–532. <https://doi.org/10.1191/0309133302pp350ra>.
- Kasse, C., Vandenberghe, D., De Corte, F., Van den Haute, P., 2007. Late Weichselian fluvio-aeolian sands and covanders of the type locality Grubbenvorst (southern Netherlands): sedimentary environments, climate record and age. *J. Quat. Sci.* 22 (7), 695–708. <https://doi.org/10.1002/jqs.1087>.
- Kindler, P., Guillevic, M., Baumgartner, M.F., Schwander, J., Landais, A., Leuenberger, M., 2014. Temperature reconstruction from 10 to 120 kyr b2k from the NGRIP ice core. *Clim. Past* 10 (2), 887–902. <https://doi.org/10.5194/cp-10-887-2014>.
- Kocurek, G., Fielder, G., 1982. Adhesion structures. *J. Sediment. Res.* 52 (4), 1229–1241. <https://doi.org/10.1306/212F8102-2B24-11D7-8648000102C1865D>.
- Konert, M., Vandenberghe, J.E.F., 1997. Comparison of laser grain size analysis with pipette and sieve analysis: a solution for the underestimation of the clay fraction. *Sedimentology* 44 (3), 523–535. <https://doi.org/10.1046/j.1365-3091.1997.d01-38.x>.
- Koster, E.A., 1988. Ancient and modern cold-climate aeolian sand deposition: a review. *J. Quat. Sci.* 3 (1), 69–83. <https://doi.org/10.1002/jqs.3390030109>.
- Küster, M., Fülling, A., Kaiser, K., Ulrich, J., 2014. Eolian sands and buried soils in the Mecklenburg Lake District, NE Germany: holocene land-use history and pedogeomorphic response. *Geomorphology* 211, 64–76. <https://doi.org/10.1016/j.geomorph.2013.12.030>.
- Lauer, T., Von Suchodoletz, H., Vollmann, H., Meszner, S., Frechen, M., Tinapp, C., Goldmann, L., Müller, S., Zielhofer, C., 2014. Landscape aridification in Central Germany during the late Weichselian Pleniglacial—results from the Zauschwitz loess site in western Saxony. *Z. Geomorphol.* 58 (1), 27–50. <https://doi.org/10.1127/0372-8854/2013/5-00163>. Supplementary Issues.
- Lehmkuhl, F., Zens, J., Krauß, L., Schulte, P., Kels, H., 2016. Loess-paleosol sequences at the northern European loess belt in Germany: distribution, geomorphology and stratigraphy. *Quat. Sci. Rev.* 153, 11–30. <https://doi.org/10.1016/j.quascirev.2016.10.008>.
- Maarleveld, G., Van der Schans, R.P.H.P., 1961. *The morphology of the cover sands in the Guelders Valley*. Tijdschrift het K. Ned. Aardrijkd. Genoot. 78, 22–34.
- Manikowska, B., 1991. Dune processes, age and dune terrace ad Vistulian decline in the Vistula valley near Wyszogród, Central Poland. *Bulletin of the Polish Academy of Sciences. Earth Sci.* 39 (2), 138–148.
- Matlakhova, E., 2015. Aeolian processes and landforms in river valleys of central Russian plain in MIS 2. European geosciences union general assembly 2015. *Geophys. Res. Abstr.* 17, 188–188.
- Moldkov, A., Bitinas, A., 2006. Sedimentary record and luminescence chronology of the Late glacial and Holocene aeolian sediments in Lithuania. *Boreas* 35, 244–254. <https://doi.org/10.1111/j.1502-3885.2006.tb01154.x>.
- Mountney, N.P., Russell, A.J., 2009. Aeolian dune-field development in a water table-controlled system: Skeidararsandur, Southern Iceland. *Sedimentology* 56 (7), 2107–2131. <https://doi.org/10.1111/j.1365-3091.2009.01072.x>.
- Murton, J.B., Bateman, M.D., Baker, C.A., Knox, R., Whiteman, C.A., 2003. The devensian periglacial record on Thanet, Kent, UK. *Permafr. Periglac. Process.* 14, 217–246. <https://doi.org/10.1002/ppp.442>.
- Nationale database flora en fauna, 2020. September 20). <https://ndff.nl>.
- Parks, D.A., Rendell, H.M., 1992. Thermoluminescence dating and geochemistry of loessic deposits in southeast England. *J. Quat. Sci.* 7 (2), 99–107. <https://doi.org/10.1002/jqs.3390070203>.
- Paterson, G.A., Heslop, D., 2015. New methods for unmixing sediment grain size data. *G-cubed* 16 (12), 4494–4506. <https://doi.org/10.1002/2015GC006070>.
- PDOK, 2020a. May 5 Geomorfol. Kaart Nederland. 1, 50000. Retrieved from. <https://PDOK.nl>.
- PDOK, 2020b. June 30). AHN2. Retrieved from. <https://PDOK.nl>.
- Pierik, H.J., van Lanen, R.J., Gouw-Bouman, M.T., Groenewoudt, B.J., Wallinga, J., Hoek, W.Z., 2018. Controls on late-Holocene drift-sand dynamics: the dominant role of human pressure in The Netherlands. *Holocene* 28 (9), 1361–1381. <https://doi.org/10.1177/0959683618777052>.
- Pons, L.J., Wiggers, A.J., 1958. De morfologie van het pleistocene oppervlak in Noord-Holland en het Zuiderzegebied, voor zover gelegen beneden gemiddeld zeeniveau (NAP). *Tijdschrift het K. Ned. Aardrijkd. Genoot.* 75, 140–153.
- Prins, M.A., Weltje, G.J., 1999. End-member modeling of siliciclastic grain-size distributions: the late Quaternary record of aeolian and fluvial sediment supply to the Arabian Sea and its paleoclimatic significance. In: Harbaugh, J. (Ed.), *Numerical Experiments in Stratigraphy: Recent Advances in Stratigraphic and Sedimentologic Computer Simulations*, Society for Sedimentary Geology. SEPM Special Publication, pp. 91–111 no. 62).
- Rains, R.B., Selby, M.J., Smith, C.J.R., 1980. Polar desert sandar, Antarctica. *N. Z. J. Geol. Geophys.* 23 (5–6), 595–604. <https://doi.org/10.1080/00288306.1980.10424131>.
- Rannik, Ü., Altimir, N., Raittila, J., Suni, T., Gaman, A., Hussein, T., Hölttä, T., Lassila, H., Latokartano, M., Lauri, A., Natsheh, A., Peltäjä, T., Sorjamaa, R., Ylä-Mella, H., Keronen, P., Berninger, F., Vesala, T., Kulmala, M., 2002. Fluxes of carbon dioxide and water vapour over Scots pine forest and clearing. *Agric. For. Meteorol.* 111 (3), 187–202. [https://doi.org/10.1016/S0168-1923\(02\)00022-9](https://doi.org/10.1016/S0168-1923(02)00022-9).
- Rasmussen, S.O., Bigler, M., Blockley, S.P., Blunier, T., Buchardt, S.L., Clausen, H.B., et al., 2014. A stratigraphic framework for abrupt climatic changes during the Last Glacial period based on three synchronized Greenland ice-core records: refining and extending the INTIMATE event stratigraphy. *Quat. Sci. Rev.* 106, 14–28. <https://doi.org/10.1016/j.quascirev.2014.09.007>.
- Renssen, H., Kasse, C., Vandenberghe, J., Lorenz, S.J., 2007. Weichselian Late Pleniglacial surface winds over northwest and central Europe: a model–data comparison. *J. Quat. Sci.* 22 (3), 281–293. <https://doi.org/10.1002/jqs.1038>.
- Schokker, J., Cleveringa, P., Murray, A.S., Wallinga, J., Westerhoff, W.E., 2005. An OSL dated middle and late quaternary sedimentary record in the roer valley Graben (southeastern Netherlands). *Quat. Sci. Rev.* 24 (20–21), 2243–2264. <https://doi.org/10.1016/j.quascirev.2005.01.010>.
- Schokker, J., Weerts, H.J.T., Westerhoff, W.E., Berendsen, H.J.A., Otter, C.D., 2007. Introduction of the Boxtel formation and implications for the quaternary lithostratigraphy of The Netherlands. *Neth. J. Geosci./Geol. Mijnbouw.* 86 (3), 197–210. <https://doi.org/10.1017/S0016774600077805>.
- Schwan, J., 1986. The origin of horizontal alternating bedding in Weichselian aeolian sands in northwestern Europe. *Sediment. Geol.* 49 (1–2), 73–108. [https://doi.org/10.1016/0037-0738\(86\)90016-3](https://doi.org/10.1016/0037-0738(86)90016-3).
- Schwan, J., 1988. The structure and genesis of Weichselian to early Holocene aeolian sand sheets in western Europe. *Sediment. Geol.* 55 (3–4), 197–232. [https://doi.org/10.1016/0037-0738\(88\)90132-7](https://doi.org/10.1016/0037-0738(88)90132-7).
- Sevink, J., Van Geel, B., Jansen, B., Wallinga, J., 2018. Early Holocene forest fires, drift sands, and Usselo-type paleosols in the Laarder Wasmeren area near Hilversum, The Netherlands: implications for the history of sand landscapes and the potential role of Mesolithic land use. *Catena* 165, 286–298. <https://doi.org/10.1016/j.catena.2018.02.016>.
- Shang, Y., Kaakinen, A., Beets, C.J., Prins, M.A., 2018. Aeolian silt transport processes as fingerprinted by dynamic image analysis of the grain size and shape characteristics of Chinese loess and Red Clay deposits. *Sediment. Geol.* 375, 36–48. <https://doi.org/10.1016/j.sedgeo.2017.12.001>.
- Stancikaitė, M., Baltrūnas, V., Karmaza, B., Karmazienė, D., Molodkov, A., Ostrauskas, T., Obukhowsky, V., Sidorowich, W., Motuzko, A., 2011. The late glacial history of gornitsa foreland and Kovaltsy palaeolithic site. *W. Belarus. Balt.* 24 (1), 25–36.
- Streeter, D., 2016. *Collins Wild Flower Guide, second ed.* HarperCollins Publishers, London.
- Tanskanen, H., Venäläinen, A., Puttonen, P., Granström, A., 2005. Impact of stand structure on surface fire ignition potential in Picea abies and Pinus sylvestris forests in southern Finland. *Can. J. For. Res.* 35 (2), 410–420. <https://doi.org/10.1139/x04-188>.
- TNO-GSN, 2021. Wierden member. In: *Stratigraphic Nomenclature of the*

- Netherlands, TNO – Geological Survey of the Netherlands. Accessed on 01-03-2021 from. <http://www.dinoloket.nl/en/stratigraphic-nomenclature/wierden-member>.
- Van Aalst, J.W., 2020. Opentopo. June 30). <https://www.opentopo.nl>.
- Van Beurden, L., 2020. Botanische macroresten voor 14C-datering van laatglaciale afzettingen aangetroffen ter hoogte van de kruising A28/N226 te Leusden. <https://doi.org/10.17026/dans-xx4-3t9d>. DANS.
- Vandenbergh, D.A.G., Derese, C., Kasse, C., Van den Haute, P., 2013. Late Weichselian (fluvio-) aeolian sediments and Holocene drift-sands of the classic type locality in Twente (E Netherlands): a high-resolution dating study using optically stimulated luminescence. *Quat. Sci. Rev.* 68, 96–113. <https://doi.org/10.1016/j.quascirev.2013.02.009>.
- Vandenbergh, J., 1988. Cryoturbations. In: Clark, M.J. (Ed.), *Advances in Periglacial Geomorphology*. Wiley, pp. 179–200.
- Van der Hammen, T., 1951. PhD Thesis. In: *Late-Glacial Flora and Periglacial Phenomena in the Netherlands*. Eduard IJdo N.V., Leiden, p. 183.
- Van der Hammen, T., Van Geel, B., 2008. Charcoal in soils of the Allerød-Younger Dryas transition were the result of natural fires and not necessarily the effect of an extra-terrestrial impact. *Neth. J. Geosci.* 87 (4), 359–361. <https://doi.org/10.1017/S0016774600023416>.
- The upper quaternary of the Dinkel valley (Twente, eastern Overijssel, The Netherlands). In: Van der Hammen, T., Wijmstra, T.A. (Eds.), *Meded. Rijks Geol. Dienst* 22, 55–213.
- Van Geel, B., Coope, G.R., Van Der Hammen, T., 1989. Palaeoecology and stratigraphy of the Lateglacial type section at Usselo (The Netherlands). *Rev. Palaeobot. Palynol.* 60 (1–2), 25–129. [https://doi.org/10.1016/0034-6667\(89\)90072-9](https://doi.org/10.1016/0034-6667(89)90072-9).
- Van Hateren, J.A., Prins, M.A., Van Balen, R.T., 2018. On the genetically meaningful decomposition of grain-size distributions: a comparison of different end-member modelling algorithms. *Sediment. Geol.* 375, 49–71. <https://doi.org/10.1016/j.sedgeo.2017.12.003>.
- Van Hateren, J.A., Van Buuren, U.V., Arens, S.M., Van Balen, R.T., Prins, M.A., 2020. Identifying sediment transport mechanisms from grain size–shape distributions, applied to aeolian sediments. *Earth Surf. Dyn.* 8 (2), 527–553. <https://doi.org/10.5194/esurf-8-527-2020>.
- Van Huissteden, J., 1990. *Tundra Rivers of the Last Glacial: Sedimentation and Geomorphological Processes during the Middle Pleniglacial in Twente, Eastern Netherlands*. Centrale Huisdrukkerij van de Vrije Universiteit, Amsterdam, p. 231.
- Van Huissteden, J.K., Vandenbergh, J., Van der Hammen, T., Laan, W., 2000. Fluvial and aeolian interaction under permafrost conditions: Weichselian Late Pleniglacial, Twente, eastern Netherlands. *Catena* 40 (3), 307–321. [https://doi.org/10.1016/S0341-8162\(00\)00085-0](https://doi.org/10.1016/S0341-8162(00)00085-0).
- Van Huissteden, K.J., Schwan, J.C., Bateman, M.D., 2001. Environmental conditions and paleowind directions at the end of the Weichselian Late Pleniglacial recorded in aeolian sediments and geomorphology (Twente, Eastern Netherlands). *Neth. J. Geosci.* 80 (2), 1–18. <https://doi.org/10.1017/S0016774600022277>.
- Van Vliet-Lanoë, B., 1989. Dynamics and extent of the Weichselian permafrost in western Europe (substage 5e to stage 1). *Quat. Int.* 3, 109–113. [https://doi.org/10.1016/1040-6182\(89\)90080-3](https://doi.org/10.1016/1040-6182(89)90080-3).
- Vorobieva, G., Vashukevich, N., Berdnikova, N., Berdnikov, I., Zolotarev, D., Kuklina, S., Lipnina, E., 2021. Soil formation, Subaerial sedimentation processes and ancient cultures during MIS 2 and the deglaciation phase MIS 1 in the Baikal–Yenisei Siberia (Russia). *Geosciences* 11 (8), 323. <https://doi.org/10.3390/geosciences11080323>.
- Weltje, G.J., Prins, M.A., 2003. Muddled or mixed? Inferring paleoclimate from size distributions of deep-sea clastics. *Sediment. Geol.* 162, 39–62. [https://doi.org/10.1016/S0037-0738\(03\)00235-5](https://doi.org/10.1016/S0037-0738(03)00235-5).
- Weltje, G.J., Prins, M.A., 2007. Genetically meaningful decomposition of grain-size distributions. *Sediment. Geol.* 202 (3), 409–424. <https://doi.org/10.1016/j.sedgeo.2007.03.007>.
- Westerink, R.M., 1981. Master thesis. In: *Geologie en geomorfologie van stuwwal, gordeldekzandgebied en Gelderse Vallei ten zuiden van Amersfoort (Geology and geomorphology of the ice-pushed ridge, coversand plateau and Gelderse Vallei south of Amersfoort)*. Amsterdam University, p. 62.
- Woolderink, H.A.G., Kasse, C., Cohen, K.M., Hoek, W.Z., Van Balen, R.T., 2019. Spatial and temporal variations in river terrace formation, preservation, and morphology in the Lower Meuse Valley, The Netherlands. *Quat. Res.* 91 (2), 548–569. <https://doi.org/10.1017/qua.2018.49>.
- Zeeberg, J.J., 1994. *The Nature and Distribution of Late Pleistocene Dunes in the European Lowlands and on the Russian Platform*. Report ICG 95/1, The Netherlands Centre for Geo-Ecological Research, Utrecht University, p. 26.
- Zeeberg, J.J., 1998. The European sand belt in eastern Europe – and comparison of Lateglacial dune orientation with GCM simulation results. *Boreas* 27, 127–139. <https://doi.org/10.1111/j.1502-3885.1998.tb00873.x>.
- Zieliński, P., Sokołowski, R.J., Woronko, B., Jankowski, M., Fedorowicz, S., Zaleski, I., Molodkov, A., Weckwerth, P., 2015. The depositional conditions of the fluvioaeolian succession during the last climate minimum based on the examples from Poland and NW Ukraine. *Quat. Int.* 386, 30–41. <https://doi.org/10.1016/j.quaint.2014.08.013>.